[American Journal of Science, Vol. 311, May, 2011, P. 404–441, DOI 10.2475/05.2011.02]

NEW AGE DATA FROM THE DZIRULA MASSIF, GEORGIA: IMPLICATIONS FOR THE EVOLUTION OF THE CAUCASIAN VARISCIDES

FRANZ MAYRINGER*,†, PETER J. TRELOAR**, AXEL GERDES***, FRITZ FINGER*, and DAVID SHENGELIA§

ABSTRACT. The Caucasus mountain belt has a complex tectono-thermal history that is as yet poorly understood due to the scarcity of reliable geochronological information. Here, we report new monazite and zircon data from the Dzirula massif in the southern Caucasus, which permit development of a model for Variscan LP-HT (low pressure–high temperature) metamorphism in this region. Data are presented for two key lithologies of the Dzirula massif: 1) a group of variably deformed granitoid (mainly granodioritic-tonalitic) rocks and 2) metapelitic LP-HT cordierite-biotite-sillimanite migmatites and paragneisses. Electron-microprobe Th-U-total Pb monazite dating demonstrates that the LP-HT metamorphism in the Dzirula massif is Variscan, and occurred around 330 Ma. LA-ICP-MS zircon dating reveals that the granitoids include two different magmatic series. An older, mainly tonalitic, series is of Lower Cambrian age. Younger intrusions, including gabbros and diorites, but mainly tonalites and granodiorites, are Variscan in age. The older series show ductile deformation features and, along with the metapelites, experienced Variscan high-grade metamorphism that resulted in penetrative blastic recrystallization and anatexis. The younger series is generally undeformed, but often shows a magmatic foliation, and variable alteration under greenschist facies conditions. It is suggested that the Variscan intrusions facilitated the regional LP-HT metamorphic event at 330 to 340 Ma. Age and petrographic data from the Greater Caucasus imply a similar evolution as observed in the Dzirula massif. The Dzirula massif can thus be used as a proxy to model the evolution of the Caucasian Variscides.

Key words: Caucasus, Variscides, Black Sea–Central Transcaucasian terrane, zircon, monazite, geochronology

INTRODUCTION

The Caucasian region of Georgia and southern Russia is commonly viewed as a part of the Variscan orogenic belt (Gamkrelidze, 1986, 1997; Adamia and others, 1987; Hanel and others, 1993a, 1993b; Somin and others, 2006). However, in comparison to the central and western European sections, this eastern continuation of the Variscan orogen is relatively poorly known. Most of the first order data from the Caucasus come from studies that predate the collapse of the Soviet Union. Published field and petrographic data are robust, but too much reliance is placed on isotopic data that use non-robust systems such as K-Ar or Rb-Sr data from altered, metamorphic rocks.

Here we summarize new petrological, geochemical, and geochronological data from the Dzirula massif in Georgia. In particular, we present laser-ablation U-Pb zircon ages and electronmicroprobe monazite Th-U-total Pb ages for two key lithologies of the massif: metapelitic Crd-Bt-Sil-migmatites and paragneisses, and variably deformed tonalitic-granodioritic rocks. These two key lithologies are widespread in the Dzirula massif, but have given rise to contrasting interpretations. The aim of this study is

* Division of Mineralogy, Salzburg University, Hellbrunnerstrasse 34, 5020 Salzburg, Austria
** Centre for Earth and Environmental Research, Kingston University, Kingston-upon-Thames, Surrey, KT1 2EE, United Kingdom
*** Institut für Geowissenschaften, Goethe Universität, 60054 Frankfurt/Main, Germany
§ A. Janelidze Geological Institute of Academy of Sciences of Georgia, Department of Mineralogy, Petrology and Geochemistry, 1/9 M. Alexide Street, 380093 Tbilisi, Georgia
† Corresponding author: Franz.Mayringer@sbg.ac.at

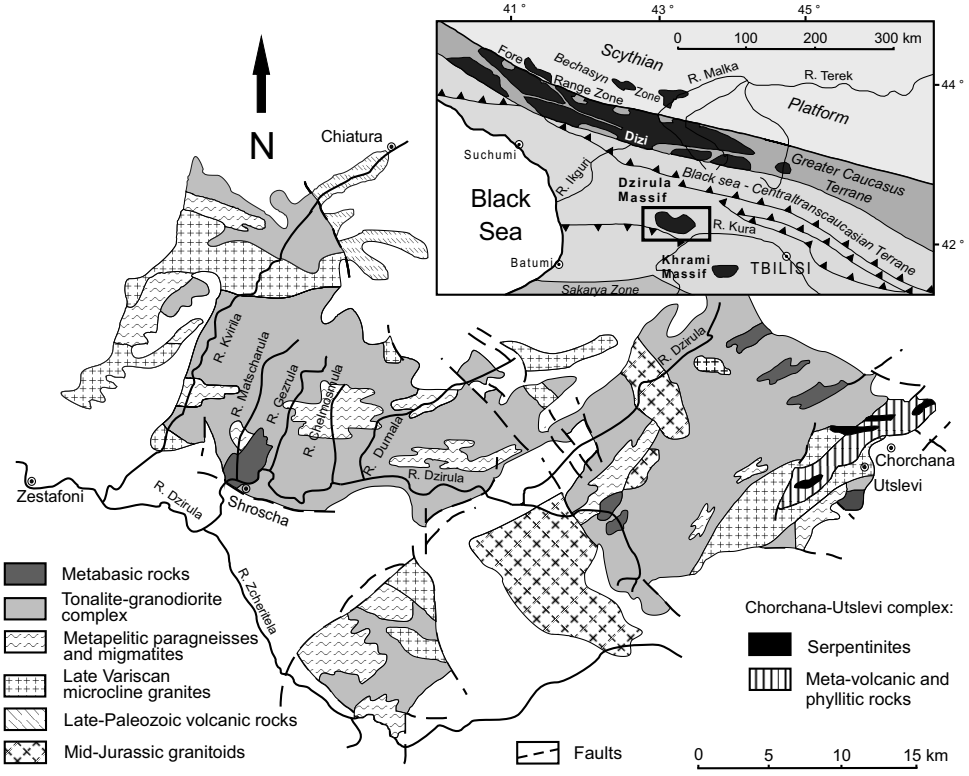

Fig. 1. Geological map of the Dzirula massif (slightly modified after Gamkrelidze and Shengelia, 2001). Inset shows the position of the massif within the tectonic framework of the Caucasus region (mainly after Gamkrelidze, 1997, with modifications taken from Moix and others, 2008).

two-fold. First is to constrain the timing and conditions of metamorphism in the Dzirula massif and to use geochemical data to characterize the magmatic rocks. Second is to compare these data with nearby parts of the Variscan orogen in order to develop a model for the evolution of the eastern end of the orogen.

TECTONIC SETTING OF THE CAUCASIAN TERRANES

Along with the rest of the Alpine-Himalayan belt the Caucasus experienced major crustal shortening during the Tertiary. Although there is little evidence of thermal overprint at this stage, important thin skinned thrust and fold belts were developed within the region (fig. 1). These make unraveling the earlier structures difficult and hence, seeing back into the Variscan period is not always easy. Nevertheless, there is wide agreement today that most of the crystalline massifs of the Caucasian area represent parts of Gondwana derived terranes that accreted to each other and the Laurussian megacontinent during Variscan orogenesis (Adamia and others, 1987; Yilmaz and others, 2000; Stampfli and Borel, 2002; Golonka, 2004; Kazmin, 2006; Bagheri and Stampfli, 2008). Basement outcrops in the north (Fore Range and Bechasyn zones) belong to the Scythian platform, which was already connected to Laurussia in pre-Variscan times.

During the Early Mesozoic Cimmerian orogeny and the closure of Palaeotethys, other Gondwanan fragments (the Cimmerian terranes) were attached to the southern edge of the Laurasian margin (Stampfli and Borel, 2002; von Raumer and others,

2003; Golonka, 2004). The southern margin of the Caucasian Variscides and its contact with the Cimmerian terranes is obscured by Triassic (Sakarya zone in fig. 1) and Jurassic oceanic basins (Moix and others, 2008; Bagheri and Stampfli, 2008) and their complex convergence. Furthermore, this area was later affected by Jurassic through Pliocene volcanic activity, which occurred most probably as a result of the northward subduction of the Neotethys (Yilmaz and others, 2000).

Terrane nomenclature in the Caucasus is not consistent, but there is wide agreement on the point that a Greater Caucasus Terrane to the north must be distinguished from a Black Sea–Central Transcaucasian Terrane or Pontian-Transcaucasian Microcontinent to the south (Gamkrelidze, 1997; Kazmin, 2006). We note that some authors (Yilmaz and others, 2000) subdivide the latter into two: the Black Sea–Central Transcaucasian Terrane in the north and a Baiburt-Sevanian terrane in the south (not shown in fig. 1). The Dizi Series of Svanetia, located along the southern slope of the Greater Caucasus (fig. 1), is commonly interpreted as a redundant Devonian oceanic domain that, prior to its closing in the Carboniferous, separated the Greater Caucasus Terrane from the Black Sea–Central Transcaucasian Terrane (Kazmin, 2006). These two terranes made contact and sutured to the Scythian platform during the Carboniferous. Considerable debate revolves around the question whether it is the Dizi suture, or the northern boundary of the Greater Caucasus terrane, which constitutes the main Variscan suture (that is, the Rhenohercynian-Prototethys suture—Stampfli and Borel, 2002).

THE DZIRULA MASSIF

The Dzirula massif, part of the Black Sea–Central-Transcaucasian terrane (fig. 1), is the largest and best studied of the pre-Alpine crystalline inliers south of the Main Range zone (Gamkrelidze, 1991; Zakariadze and others, 1998, 2007; Gamkrelidze and Shengelia, 1999, 2001). Geological maps of the massif have been published by Gamkrelidze and Shengelia (2001) and Zakariadze and others (2007). These maps differ significantly from each other. The map differences are most likely due to poor exposure and contacts that are difficult to define in the field. Our fieldwork, involving re-mapping of key road and river sections, leads us to favor the interpretation of Gamkrelidze and Shengelia (2001). We do not recognize many of the features mentioned by Zakariadze and others (2007). As outlined below, we suspect that this is because we focused on the Dzirula massif alone, whereas Zakariadze and others (2007) attempted to force a unified stratigraphy that covers more than one tectonic inlier that we argue should each be considered separately.

We identified a number of key lithologies within the Dzirula massif (fig. 1). The first is a series of variably deformed and metamorphosed biotite ± hornblende-bearing tonalites and granodiorites, some of which contain mafic enclaves. These rocks have previously been described and mapped as quartz-diorites and quartz-diorite gneisses (Gamkrelidze and Shengelia, 2001). However the quartz content, at generally >20 percent, is too high for a quartz-diorite or monzo-diorite. In our sketch map in figure 1, we label these rocks as tonalite-granodiorite complex. Our field data support the view of Gamkrelidze and Shengelia (2001) that rocks of this kind cover a large part of the Dzirula massif and represent the dominant lithology in the inlier. Some units mapped separately by Gamkrelidze and Shengelia (2001) as "microclinized granite-gneiss and migmatite," along the Dzirula-valley, have also been included by us in the tonalite-granodiorite complex because according to our field observations, they represent essentially the same rock types. We do not follow the interpretations of Gamkrelidze and Shengelia (2001) that these rocks originated by large scale K-metasomatism. Although we found in places alteration by low-T processes and an intensive penetration by granitic, aplitic and pegmatitic dike swarms originated from the late Variscan

Pink Granite intrusions (see below), we see no evidence to support penetrative metasomatic chemical alteration of the rocks.

The tonalite-granodiorite complex previously yielded a variety of poorly constrained dates including U-Pb zircon ages of 491 $+93/-36$ Ma (Barnitsky and others, 1990), Sm-Nd ages of 607 $\pm$ 78 Ma (Zakariadze and others, 1998, 2007) and Rb-Sr ages of 686 $\pm$ 54 Ma and 532 $\pm$ 63 Ma (Okrostsvaridze and others, 2002). The large errors on these data are a cause for concern. The rocks have experienced a Variscan thermal event (see below), have resided in the hanging wall of a Jurassic subduction zone and are often extensively hydrated. Thus the significance of these published ages appears questionable.

A second key lithology is a series of cordierite-biotite-sillimanite-bearing metasediments (mainly metapelites and metagraywackes) that show evidence for partial melting. These metapelitic paragneisses and migmatites occur as enclaves (rafts or screens) within the tonalite-granodiorite complex (fig. 1). The LP-HT (low pressure–high temperature) granulite facies metamorphism recorded in the metapelites is reported for the first time as being Variscan in age.

Mafic sheets of various ages are exposed within both of these units (fig. 1). Some of these experienced the same LP-HT metamorphic history as the metapelites and must therefore be pre-Variscan. Other units, for example the Shroscha basic massif, intruded into the metamorphic complex, and may therefore be considered Variscan intrusives.

The third major lithological type is a series of pink, biotite-bearing, I-type microcline granites. The pink granites yield K-Ar muscovite and biotite ages of between 300 and 340 Ma with a statistical mean of 321 $\pm$ 6 Ma (Dudauri and others, 1990). They document a late Variscan thermal event to which the metagranitoid complex and the metapelites were exposed.

The massif also hosts a greenschist facies sequence of basic rocks, low grade clastic metasediments, and serpentinites (the Chorchana-Utslevi belt; Tsutsunava, 2002). The serpentinites have been interpreted as an ophiolitic sliver. A Sm-Nd "isochron" dates this sequence, faunally constrained as Cambrian in age, at 804 $\pm$ 100 Ma (Zakariadze and others, 2007). On the basis of the faunal data it is hard to place any reliance on this radiometric age.

The Dzirula massif is unconformably overlain by unmetamorphosed volcaniclastic rocks, dominated by rhyolitic and rhyo-dacitic tuffs, with a late Palaeozoic (Bashkirian) age of ~300 Ma (Dudauri and others, 1990). These rocks are well exposed along the northern margin of the massif near Chiatura. Zakariadze and others (2007) overestimate the extent of this volcanic unit. Their map shows that these rocks crop out over large areas north of the Dzirula valley. Our fieldwork did not confirm this.

Our lithological interpretation of the Dzirula massif is significantly different from that of Zakariadze and others (1998, 2007) in other respects. They identify a Late Proterozoic to Early Palaeozoic "oldest oceanic basement unit," a Neo-Proterozoic to Cambrian Grey Granite basement unit (volcanic arc), and a Microcline Granite basement complex. We do not recognize these subdivisions from our fieldwork. The Microcline Granite Basement complex is readily identified as identical to our pink granites, which show a variety of magmatic fabrics. The gray granite basement complex is broadly the equivalent of our tonalite-granodiorite complex with occasional gabbroic bodies. However, Zakariadze and others (2007) fail to recognize the presence of both deformed and undeformed varieties. Our age data, presented below, suggest that many of the magmatic bodies included within the "Grey Granite unit" are much younger than Cambrian in age. Zakariadze and others (2007) do not mention the presence of LP-HT cordierite-sillimanite migmatites and paragneisses, and we have seen no evidence for the low-grade metamorphic rocks described by them. However,

we have a major concern with the map presented by Zakariadze and others (2007) where it relates to their "oldest basement unit." The description of this unit as oceanic crust leans largely on poor exposures of rocks from the Lokhi massif. On its western margin, the Lokhi massif is flanked by a series of thrust packages that contain low-temperature metamorphic rocks and magmatic rocks with an apparent oceanic affinity (Gamkrelidze and others, 1999). It is possible that these represent a late Proterozoic ophiolitic assemblage. However, within the Dzirula massif, the only potential ophiolitic rocks are contained within the Cambrian-aged Chorchana-Utslevi belt. These were tectonically intercalated within the Dzirula massif most likely during the Variscan.

Furthermore, we observed that areas mapped as an oldest oceanic basement unit by Zakariadze and others (2007) actually contain a large number of granitoid rocks, identified by Gamkrelidze and Shengelia (2001) mainly as quartz-diorite gneiss. We note that these quartz-diorite gneisses (belonging to the tonalite-granodiorite complex in the terminology of the present study) are not the equivalent of the "grey granite basement complex" of Zakariadze and others (2007) as one might conclude from the names at first glance. Comparison of the two existing maps shows that the "grey granite basement complex" of Zakariadze and others (2007) matches up more or less with the relatively small metabasic bodies in the map of Gamkrelidze and Shengelia (2001) that is the basic massif near Shroscha and the basic rocks mapped in the eastern part of the Dzirula massif (fig. 1).

PETROGRAPHY OF THE TONALITE-GRANODIORITE COMPLEX

We have studied the tonalite-granodiorite complex along profiles following the Dzirula, Matscharula, Gezrula, Dumala, Kvirila and Chelmosmula Rivers and at the eastern margin of the massif, close to the Chorchana-Utslevi belt (fig. 1). The rocks are variably deformed and are mostly tonalitic to granodioritic in bulk composition. Quartz-diorites, dioritic-gabbros and granites form minor parts of the sequence. The granitoids contain significant amounts (10 to 15%) of biotite (often partially replaced by chlorite) and minor hornblende (often replaced by actinolite and/or chlorite). Plagioclase compositions in tonalitic-granodioritic varieties are generally $An_{20\text{ to }40}$. Crystal size is generally 1 to 5 mm. The granitoids are commonly gray in color, although a red to pink color can be observed in other places, which is partly due to low-T alteration processes (hematitization), attributed to contact metamorphic phenomena with nearby bodies of pink granites and their dike swarms. Figure 2 shows the macroscopic variability of the metagranitoid rocks.

Our field work enables us to divide the complex into two units on the basis of deformation state. Some of the tonalites and granodiorites show high-T deformation with variable development of a gneissic fabric dominantly defined by segregation of aligned biotite crystals and feldspars. Although few are strongly deformed, tectonic fabrics are clearly developed, locally by mafic enclaves stretched parallel to the tectonic fabric. The deformed rocks locally show evidence for anatexis. By contrast, the undeformed tonalites and granodiorites show magmatic fabrics and no blastesis or evidence for anatexis, and we interpret them to be intrusive into the deformed set. Our interpretation is supported by our new geochronological data reported below.

Both the older and the younger granitoid units contain mafic enclaves. These are mostly fine-grained dioritic rocks. The shape of the enclaves can vary from nearly round (20-30 cm) to mostly elongate (20 cm-1 m long). Due to the presence of magma mingling phenomena, we interpret these dioritic enclaves as coexisting mafic magmas and not as roof pendants or relicts of older crust. Mafic enclaves representing coeval magma, that either did not or did partially mix with the granitic host, are typical of many tonalitic-granodioritic I-type suites all over the world (Barbarin, 1999).

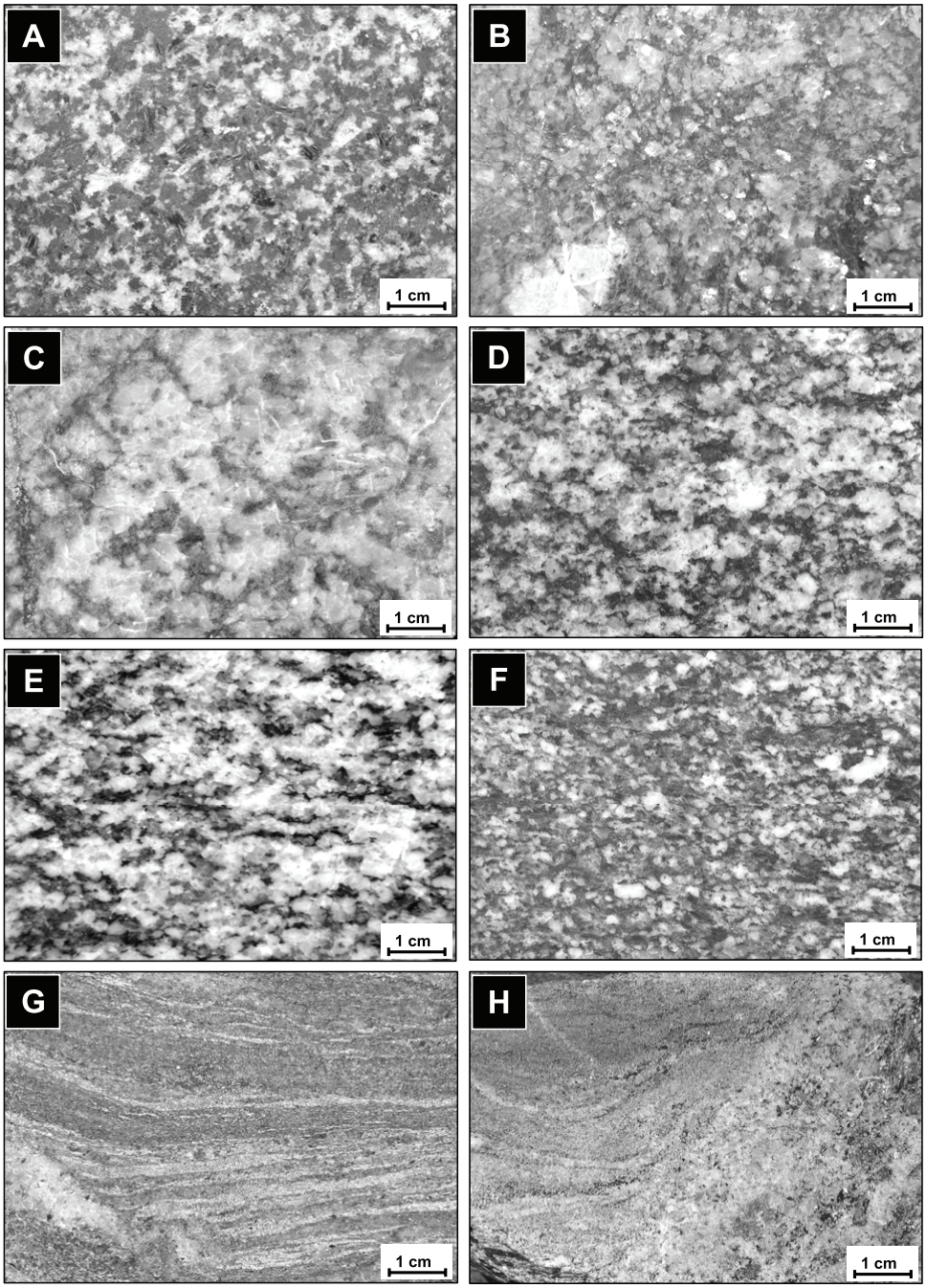

Fig. 2. Major rock types of the Dzirula massif: (A) gabbro from Shroscha (GE0132); (B-D) Variscan intrusive rocks from the tonalite-granodiorite complex (GE0127, GE0164, GE0345); (E-F): pre-Variscan granitoids from the tonalite-granodiorite complex (GE0011, GE0347); (G-H) anatectic metapelites.

There are two petrographic indicators to differentiate the older (high-grade metamorphic) and younger intrusive groups of granitoids. The first is the plagioclase.

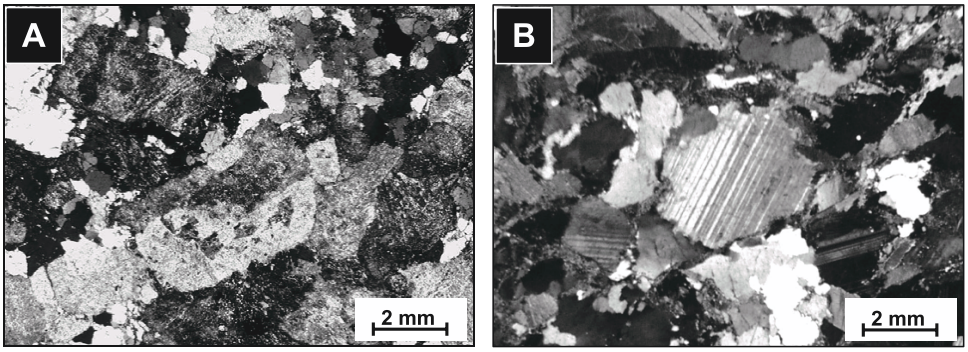

Fig. 3. Thin-section photographs (crossed polarizers) showing the igneous fabric of a Variscan tonalite with euhedral Carlsbad twinned plagioclases (A: sample GE0164) compared to the metablastic feldspar fabric common to the older group of granitoids (B: sample GE0011).

Plagioclase forms round, 1 to 5 mm sized porphyroblasts in the older metagranitoids, whereas plagioclase occurs as euhedral to subhedral magmatic crystals, with Carlsbad twinning and locally faint oscillatory magmatic zoning in the younger granitoids (fig. 3). In the younger granitoids, plagioclase is often strongly seriticized, obscuring the magmatic textures. A second diagnostic mineral is zircon. In cathodoluminescence images zircon displays metamorphic overgrowth rims in the older metagranitoid unit, and undisturbed igneous growth textures (that is, oscillatory zoning) in the younger granitoid unit (see section on zircon dating below).

PETROGRAPHY OF THE METAPELITES

The outcrop pattern of the metapelites is poorly defined, due to poor exposure in central Georgia. Our field data suggest that the metapelites form screens of metasedimentary material between the tonalitic and granodioritic rocks. We sampled the metapelites along the valleys of the Dzirula, Kvirila, Matscharula, Gezrula, Dumala, and Chelmosmula Rivers (fig. 1). The metapelites are mostly fine-grained biotite- and quartz-rich, muscovite-poor rocks with variable feldspar contents. In outcrop, they appear both as stromatic migmatites (metatexites) and as diatexite migmatites (fig. 2G-H). In leucosome-rich exposures, schlieren of mica schist form rafts of material contained within a granitic neosome. Most leucosome layers within the mica schists are bounded by mafic selvages rich in biotite. No primary muscovite was observed suggesting that the melt reaction was a biotite fluid-absent one occurring at temperatures greater than that of muscovite breakdown in the presence of quartz.

In thin section, the metapelites display cordierite porphyroblasts up to 3 mm in diameter (fig. 4). Cordierite is generally strongly pinitized and replaced by secondary muscovite and green biotite. K-feldspar is commonly present together with cordierite. Occasionally, needles of prismatic sillimanite can be observed (fig. 4). The mineral paragenesis indicates high-temperature, low-pressure conditions of metamorphism and melting, likely accommodated by the reaction: biotite + sillimanite + quartz $\rightarrow$ K-feldspar + cordierite + melt. Garnet is rarely present and occurs only in leucosome-poor biotite schists with an assumed graywacke protolith.

PETROGRAPHY OF THE PINK GRANITES

The late-stage pink granites are coarse-grained and consist mainly of microcline, plagioclase, and quartz. Mafic phases, normally biotite and rare hornblende, constitute $<$10 percent of the mode. Accessory minerals are apatite, zircon, and allanite. Crystal

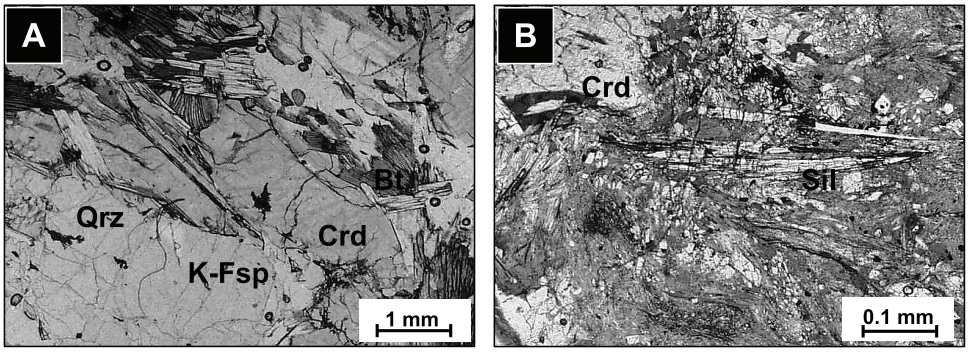

Fig. 4. Cordierite–K-feldspar–biotite–quartz (A) and cordierite-sillimanite assemblage (B) in metapelite from the Dzirula massif (sample GE0151).

size of quartz and feldspar is generally up to 4 to 5 mm, although some microcline megacrysts are up to 3 to 4 cm long. Feldspars are frequently extensively hydrated (sericitic), and biotite is overprinted by chlorite. The pink granites show a wide variety of fabrics ranging from isotropic, massive K-feldspar mega-crystic granites to variants with strong magmatic layering defined by variations in biotite content and the size of microcline phenocrysts. These features indicate emplacement as high level granite bodies.

GEOCHRONOLOGY

Analytical Procedures

The U-Th-Pb isotopic analyses (table 1) were performed at the Institute of Geosciences at Goethe University Frankfurt (GUF), Germany, using a Thermo-Scientific Element II sector field ICP mass spectrometer (SF-ICP-MS) coupled to a New Wave UP213 ultraviolet laser system (Gerdes and Zeh, 2006, 2009). A teardrop-shaped, low-volume laser cell was used to enable sequential sampling of heterogeneous grains during time-resolved data acquisition (see also Janousek and others, 2006).

Zircon spot selection (30 μm crater size) was guided by internal structures as observed in cathodoluminescence (CL) images of polished and mounted grains. Each analysis consisted of approximately 20 s background acquisition followed by 35 s data acquisition. The ^{204}Pb signal interferes with the ^{204}Hg isotope that occurs together with ^{202}Hg in the argon carrier gas. The precise detection of ^{204}Pb was therefore dependent on accurate monitoring of Hg. A common-Pb correction based on the calculated ^{204}Pb and a model Pb composition (Stacey and Kramers, 1975) was carried out when necessary. The necessity of the correction was judged on whether the corrected ^{207}Pb/^{206}Pb lay outside of the internal errors of the measured ratios. Raw data were corrected for background signal, common Pb, laser-induced elemental fractionation, instrumental mass discrimination, and time-dependant elemental fractionation of Pb/Th and Pb/U using an Excel® spreadsheet program. Reported errors (1σ on ratios, 2 σ on ages) were propagated with the reproducibility (1 s.d.) of the GJ-1 standard (n=12) over the entire session. Errors were 0.6 percent and 0.7 percent for the ^{207}Pb/^{206}Pb and ^{206}Pb/^{238}U ratios, respectively. Concordia diagrams (2σ error ellipses) and dates (95% confidence level) were produced using Isoplot/Ex 2.49 (Ludwig, 2000).

Monazite analysis followed the routine established at the Mineralogical Department of Salzburg University (Finger and Broska, 1999). This involves a complete WDS

TABLE 1

Results of zircon dating

Grain spot	$^{207}Pb^{a}$ (cps)	U^{b} (ppm)	Pb^{b} (ppm)	$^{206}Pb/^{204}Pb$	Th^{c}/U	$^{206}Pb^{c}/^{238}U$	1 σ (%)	$^{207}Pb^{c}/^{235}U$	1 σ (%)	rho[d]	$^{207}Pb^{c}/^{206}Pb$	1 σ (%)	$^{207}Pb/^{235}U$	2 σ (Ma)	$^{206}Pb/^{238}U$	2 σ (Ma)	$^{207}Pb/^{206}Pb$	2 σ (Ma)
Tonalite-gneiss (sample GE0011)																		
1.1	2612	275	23	1659	0.86	0.0809	1.4	0.6392	2.0	0.68	0.0573	1.5	502	20	501	14	504	15
4.1	3637	348	31	4873	0.75	0.0868	1.7	0.7044	2.3	0.72	0.0588	1.6	541	25	537	18	561	18
4.2	3868	378	31	2184	0.66	0.0796	1.4	0.6431	2.1	0.69	0.0586	1.5	504	21	494	14	552	16
4.3	2815	104	15	809	0.84	0.1218	1.5	1.3577	2.2	0.65	0.0809	1.7	871	39	741	21	1218	42
5.1	3239	311	30	1325	1.30	0.0885	1.4	0.7118	2.0	0.67	0.0583	1.5	546	22	547	15	542	16
8.1	4587	450	41	30520	1.02	0.0870	1.3	0.6916	1.6	0.80	0.0577	1.0	534	17	537	14	518	10
8.2	1919	327	16	18621	0.03	0.0533	1.2	0.3909	1.7	0.69	0.0532	1.3	335	12	334	8	339	9
9.1	2951	287	22	3747	0.75	0.0714	1.3	0.5701	1.9	0.73	0.0579	1.3	458	17	444	12	527	13
9.2	1161	100	8	1821	0.44	0.0731	1.5	0.5898	2.8	0.52	0.0585	2.4	471	26	455	13	548	26
10.1	4218	253	26	519	1.10	0.0882	1.5	0.7420	2.3	0.67	0.0610	1.7	564	26	545	17	641	22
12.1	4924	220	46	6898	2.32	0.1635	2.0	1.6012	2.5	0.83	0.0710	1.4	971	48	976	40	958	26
13.1	2079	231	19	3661	0.96	0.0782	1.5	0.6409	2.4	0.62	0.0594	1.9	503	24	485	15	583	22
13.2	3550	356	27	162641	0.76	0.0724	2.0	0.5783	2.4	0.84	0.0579	1.3	463	22	451	18	527	14
14.1	1541	247	13	4580	0.19	0.0538	1.2	0.3975	2.5	0.50	0.0536	2.1	340	17	338	8	355	15
15.1	2048	209	19	2737	1.06	0.0761	1.4	0.6083	2.0	0.70	0.0580	1.4	483	19	473	13	530	15
18.1	3350	250	19	1037	0.73	0.0654	1.8	0.5206	2.5	0.69	0.0578	1.8	426	22	408	14	521	19
19.1	2157	213	18	83689	1.01	0.0775	1.2	0.6225	1.6	0.80	0.0583	0.9	491	15	481	12	540	10
21.1	3297	346	29	6248	0.81	0.0803	1.4	0.6445	1.7	0.83	0.0582	1.0	505	17	498	14	537	10
21.2	3987	361	33	2270	0.87	0.0866	1.5	0.6997	2.0	0.73	0.0586	1.4	539	22	536	16	551	15
22.1	1031	110	10	2976	0.98	0.0835	1.2	0.6643	2.0	0.58	0.0577	1.6	517	21	517	12	518	17
22.2	3058	310	26	7462	0.80	0.0817	1.4	0.6517	1.8	0.78	0.0579	1.1	510	19	506	14	525	12
24.1	3740	343	29	2446	0.84	0.0802	1.3	0.6450	1.9	0.69	0.0584	1.4	505	19	497	13	543	15
25.1	1458	152	13	4875	0.50	0.0884	1.3	0.7080	1.9	0.66	0.0581	1.4	544	21	546	14	533	15
26.1	1036	174	9	0	0.17	0.0546	1.4	0.4069	2.4	0.59	0.0541	1.9	347	16	342	10	374	14
26.2	1882	197	18	6553	0.89	0.0869	1.5	0.6877	1.9	0.79	0.0574	1.1	531	20	537	16	506	12
26.3	1399	161	10	13620	0.61	0.0580	1.5	0.4387	2.4	0.64	0.0548	1.8	369	18	364	11	406	15

Table 1
(continued)

Grain spot	$^{207}Pb^{a}$ (cps)	U^{b} (ppm)	Pb^{b} (ppm)	$^{206}Pb/^{204}Pb$	Th^{c}/U	$^{206}Pb^{c}/^{238}U$	1 σ (%)	$^{207}Pb^{c}/^{235}U$	1 σ (%)	rho[d]	$^{207}Pb^{c}/^{206}Pb$	1 σ (%)	$^{207}Pb/^{235}U$	2 σ (Ma)	$^{206}Pb/^{238}U$	2 σ (Ma)	$^{207}Pb/^{206}Pb$	2 σ (Ma)
Granodiorite (sample GE0127)																		
1.1	15109	392	31	1501	0.57	0.0706	2.4	0.5433	2.6	0.92	0.0558	1.0	441	23	440	21	444	9
2.1	6406	271	14	1364	0.43	0.0514	1.5	0.3792	2.0	0.78	0.0535	1.2	326	13	323	10	352	9
3.1	8608	314	19	4336	0.26	0.0591	2.1	0.4498	2.4	0.87	0.0552	1.1	377	18	370	15	419	10
4.1	4020	155	8	1062	0.53	0.0471	1.2	0.3655	2.1	0.60	0.0563	1.6	316	13	297	7	463	15
5.1	8550	352	21	2102	0.70	0.0528	1.5	0.3820	1.9	0.77	0.0524	1.2	329	13	332	10	304	8
6.1	22547	196	20	8617	0.76	0.0519	1.4	0.3840	1.7	0.83	0.0536	0.9	330	11	326	9	355	7
7.1	1900	82	4	1657	0.38	0.0506	1.2	0.3677	1.9	0.65	0.0527	1.4	318	12	318	8	317	9
7.2	2507	115	6	2848	0.43	0.0504	1.0	0.3674	1.7	0.60	0.0529	1.4	318	11	317	7	325	9
8.1	9941	145	24	65116	1.34	0.1284	1.3	1.1297	1.8	0.75	0.0638	1.2	768	28	779	21	736	18
9.1	4531	199	11	5650	0.35	0.0516	1.3	0.3757	1.7	0.73	0.0528	1.2	324	11	325	8	319	8
10.1	5216	175	11	23163	0.36	0.0609	4.0	0.4634	4.2	0.95	0.0552	1.3	387	32	381	30	419	11
11.1	2938	144	8	24642	0.72	0.0455	1.2	0.3305	1.9	0.66	0.0526	1.4	290	11	287	7	313	9
12.1	6872	295	17	15027	0.58	0.0533	1.1	0.3898	1.7	0.64	0.0531	1.3	334	11	335	7	332	9
13.1	6872	295	17	15027	0.61	0.0533	1.1	0.3910	1.7	0.65	0.0532	1.3	335	11	335	7	338	9
14.1	6389	215	14	7117	0.35	0.0625	1.7	0.4709	2.3	0.76	0.0546	1.5	392	18	391	14	396	12
15.1	8564	243	13	9033	0.32	0.0521	1.9	0.3802	2.4	0.81	0.0529	1.4	327	15	327	12	325	9
16.1	4930	215	12	2446	0.69	0.0508	1.2	0.3790	1.9	0.64	0.0541	1.4	326	12	320	8	374	11
18.1	12775	172	11	3995	0.92	0.0502	2.0	0.3659	3.1	0.63	0.0528	2.4	317	20	316	12	322	15
19.1	6601	186	18	2440	0.36	0.0958	1.6	0.8124	2.5	0.64	0.0615	1.9	604	30	590	19	656	25
20.1	3100	122	7	1784	0.56	0.0507	1.6	0.3716	2.4	0.65	0.0532	1.8	321	16	319	10	335	12
Leuco-Quartz-diorite (sample GE0164)																		
1.1	4383	207	12	2959	0.52	0.0524	1.4	0.3876	1.8	0.79	0.0537	1.1	333	12	329	9	357	8
2.1	4874	226	12	8863	0.32	0.0529	1.5	0.3883	1.9	0.77	0.0532	1.2	333	13	332	10	339	8
3.1	3090	150	8	23914	0.46	0.0527	1.5	0.3797	2.1	0.71	0.0522	1.4	327	13	331	10	296	9
4.1	2178	109	6	2325	0.35	0.0503	1.4	0.3633	2.0	0.69	0.0524	1.5	315	13	316	9	302	9
5.1	2956	140	8	14098	0.64	0.0494	1.4	0.3584	1.9	0.75	0.0527	1.2	311	12	311	9	314	8
6.1	6292	293	15	5985	0.36	0.0509	1.4	0.3706	1.8	0.77	0.0528	1.1	320	11	320	9	321	7

TABLE 1
(continued)

Grain spot	$^{207}Pb^{a}$ (cps)	U^{b} (ppm)	Pb^{b} (ppm)	$^{206}Pb/^{204}Pb$	Th^{c}/U	$^{206}Pb^{c}/^{238}U$	1 σ (%)	$^{207}Pb^{c}/^{235}U$	1 σ (%)	rho[d]	$^{207}Pb^{c}/^{206}Pb$	1 σ (%)	$^{207}Pb/^{235}U$	2 σ (Ma)	$^{206}Pb/^{238}U$	2 σ (Ma)	$^{207}Pb/^{206}Pb$	2 σ (Ma)
Leuco-Quartz-diorite (sample GE0164)																		
1.1	15109	392	31	1501	0.57	0.0706	2.4	0.5433	2.6	0.92	0.0558	1.0	441	23	440	21	444	9
7.1	8179	358	21	39156	0.42	0.0566	1.4	0.4193	1.6	0.84	0.0537	0.9	356	12	355	10	360	6
8.1	4957	237	13	18981	0.50	0.0515	1.4	0.3759	1.7	0.79	0.0529	1.1	324	11	324	9	324	7
9.1	1652	39	4	1120	0.85	0.0888	1.4	0.7382	2.6	0.55	0.0603	2.2	561	29	548	16	615	27
10.1	12264	366	30	21202	0.33	0.0790	1.3	0.6236	1.7	0.81	0.0572	1.0	492	16	490	13	500	10
11.1	3836	179	10	10688	0.33	0.0529	1.3	0.3944	1.9	0.70	0.0541	1.4	338	13	332	9	374	10
12.1	1957	91	4	5865	0.32	0.0487	1.3	0.3544	1.9	0.70	0.0528	1.4	308	12	306	8	320	9
13.1	2254	106	5	3493	0.37	0.0490	1.3	0.3569	2.1	0.63	0.0528	1.6	310	13	308	8	321	10
14.1	15824	173	10	1710	0.46	0.0427	1.6	0.3195	3.1	0.52	0.0543	2.7	281	17	269	9	383	20
14.2	15824	173	36	3082	0.32	0.1980	1.8	3.0995	2.1	0.85	0.1136	1.1	1433	61	1164	42	1857	41
15.1	2819	131	7	1516	0.52	0.0526	1.4	0.3856	2.2	0.65	0.0532	1.7	331	15	330	9	338	11
17.1	5126	237	14	2782	0.90	0.0511	1.4	0.3702	2.0	0.71	0.0526	1.4	320	13	321	9	310	9
18.1	17809	290	33	3162	0.24	0.1140	3.5	0.9547	3.8	0.92	0.0607	1.5	681	52	696	49	630	19
19.1	7634	237	18	10068	0.42	0.0757	1.8	0.6011	2.2	0.84	0.0576	1.2	478	21	470	17	515	12
20.1	9229	294	23	10939	0.57	0.0730	1.5	0.5643	1.9	0.79	0.0561	1.2	454	17	454	14	456	11
Granodiorite-gneiss (sample GE0345)																		
1.1	905	74	8	2234	1.61	0.0900	1.2	0.7271	2.1	0.58	0.0586	1.7	555	24	556	14	552	19
1.2	4517	360	35	12171	1.23	0.0879	1.5	0.7186	1.9	0.77	0.0593	1.2	550	21	543	16	578	14
1.3	1407	233	12	990	0.32	0.0536	1.2	0.3985	2.0	0.61	0.0539	1.6	341	13	337	8	366	11
2.1	1189	168	10	488	0.99	0.0537	1.4	0.4011	2.5	0.57	0.0542	2.0	342	17	337	10	377	15
3.1	1133	190	10	25485	1.02	0.0522	1.2	0.3788	2.0	0.62	0.0526	1.5	326	13	328	8	313	10
3.2	943	155	8	64574	0.94	0.0514	1.4	0.3823	2.6	0.53	0.0539	2.2	329	17	323	9	367	16
4.1	1315	211	11	1511	0.67	0.0531	1.3	0.3855	1.9	0.66	0.0527	1.5	331	13	334	8	314	9
5.1	2453	375	22	5027	0.84	0.0573	1.2	0.4197	1.6	0.73	0.0531	1.1	356	12	359	8	334	7
7.1	678	103	6	2026	0.86	0.0525	1.5	0.3979	2.4	0.62	0.0550	1.9	340	16	330	10	413	16
8.1	2420	402	22	7350	0.81	0.0520	1.3	0.3806	2.0	0.64	0.0531	1.6	328	13	327	9	334	10

TABLE 1
(continued)

Grain spot	$^{207}Pb^a$ (cps)	U^b (ppm)	Pb^b (ppm)	$^{206}Pb/^{204}Pb$	Th^c/U	$^{206}Pb^c/^{238}U$	1 σ (%)	$^{207}Pb^c/^{235}U$	1 σ (%)	rho[d]	$^{207}Pb^c/^{206}Pb$	1 σ (%)	$^{207}Pb/^{235}U$	2 σ (Ma)	$^{206}Pb/^{238}U$	2 σ (Ma)	$^{207}Pb/^{206}Pb$	2 σ (Ma)
Granodiorite-gneiss (sample GE0345)																		
1.1	15109	392	31	1501	0.57	0.0706	2.4	0.5433	2.6	0.92	0.0558	1.0	441	23	440	21	444	9
9.1	898	137	8	1324	0.79	0.0539	1.2	0.4011	2.1	0.59	0.0540	1.7	342	14	338	8	371	13
10.1	441	72	4	1348	0.62	0.0508	1.5	0.3828	2.6	0.56	0.0547	2.2	329	17	319	9	399	17
11.1	1157	195	11	4363	0.99	0.0520	1.2	0.3773	1.9	0.65	0.0526	1.5	325	12	327	8	313	9
12.1	11558	619	51	2224	4.81	0.0421	1.5	0.3366	1.7	0.85	0.0580	0.9	295	10	266	8	531	10
12.2	2232	245	14	966	0.54	0.0536	1.6	0.4010	2.7	0.61	0.0542	2.1	342	18	337	11	381	16
13.1	3796	551	29	2171	0.49	0.0532	1.6	0.3980	2.4	0.66	0.0543	1.8	340	16	334	11	382	14
14.1	1965	263	14	5337	0.33	0.0530	1.6	0.4112	2.8	0.58	0.0563	2.3	350	20	333	11	463	21
22.1	2237	369	20	3742	0.86	0.0527	1.3	0.3994	2.3	0.56	0.0550	1.9	341	15	331	8	410	15

Sample locations: GE0011: roadcut, 3.5 km east of Shroscha; GE0127: roadcut, Shroscha; GE0164: river outcrop, Kvirila River, 6.2 km north of Dzirula River; GE0345: river outcrop, Gezrula River, 1.8 km north of Dzirula River.

(a) Within run background-corrected mean ^{207}Pb signal in counts per second.

(b) U and Pb content and Th/U ratio were calculated relative to GJ-1 reference (LA-ICP-MS values, Gerdes, unpublished).

(c) Corrected for background, within-run Pb/U fractionation and common Pb using Stacy and Kramers (1975) model Pb composition and subsequently normalized to GJ-1 reference (ID-TIMS value/measured value); $^{207}Pb/^{235}U$ calculated using $^{207}Pb/^{206}Pb/(^{238}U/^{206}Pb*1/137.88)$.

(d) Rho is the error correlation defined as $err^{206}Pb/^{238}U/err^{207}Pb/^{235}U$.

monazite analysis for elements Si, P, La, Ce, Pr, Nd, Sm, Gd, Dy, Y, Th, U, Ca and Pb. Prolonged counting times for Th (50 s), U (50 s) and Pb (400 s) enable the calculation of moderately precise Th-U-total Pb ages, following the method of Montel and others (1996). The analytical errors for a single point analysis typically correspond to a ~20 to 60 Ma error on the age (2σ). A weighted mean date with reduced error can be calculated from a larger number of measurements in a single coherent age population (Williams and others, 2006). A detailed description of standards, element X-ray lines, counting times, background positions, and interference corrections *et cetera,* used in the Salzburg microprobe laboratory for Th-U-total Pb monazite dating, is presented in Krenn and others (2008).

The Tonalite-Granodiorite Complex

Sample GE0011 (fig. 2E) is representative of the older, gneissic domain within the tonalite-granodiorite complex. CL images of the zircon grains (fig. 5A) display wide oscillatory-zoned interiors that are marginally resorbed and overgrown by variable thick outer shells interpreted as metamorphic or anatectic overgrowths (Corfu and others, 2003). Most analyses in the oscillatory-zoned inner domains provide $^{207}Pb/^{206}Pb$ ages between 500 and 550 Ma, pointing to a Cambrian igneous zircon population (table 1, fig. 6A). The outer overgrowth shells are considerably younger. Three concordant U-Pb analyses provide a concordia age of 338 ± 5 Ma considered as the age of the metamorphic overgrowth stage (fig. 6B). Due to the effects of Pb loss, data for the igneous zircon domains are often discordant, with U-Pb dates varying between 550 and 400 Ma. However, the age of the igneous zircon population can be estimated via a discordia chord intersecting with the concordia curve at 538 +22/−16 Ma (fig. 6A). A concordia age calculated with the six uppermost points of this discordia gives 540 ± 6 Ma (fig. 6B) and is considered to represent the best estimate of the magmatic formation age of the rock. Two inherited cores have $^{207}Pb/^{206}Pb$ ages of >600 Ma (table 1).

Zircon grains from three tonalite-granodiorite samples with igneous feldspars were subjected to LA-ICP-MS dating. Zircon grains in these samples are euhedral and display a magmatic oscillatory zoning in BSE images, which continues into the grain margins (figs. 5B-C). Metamorphic rims are not visible, but some zircon grains contain large inherited cores. Laser analyses indicate a Variscan age for the zircon populations of all three samples (figs. 6C-H). Only spots placed within inherited cores resulted in significantly older (early Palaeozoic and late Precambrian) ages. A few analyses are affected by Pb-loss. Attempts to calculate concordia ages provide dates of 325 ± 3 Ma, 328 ± 4 Ma and 331 ± 3 Ma, respectively (figs. 6D, F, H). These dates are considered as intrusion ages, and point to an important plutonic event in the Dzirula massif.

Monazite is generally rare in the tonalite-granodiorite complex. When present, microprobe dates are mostly Variscan in age (table 2). This holds true for both the older high-grade metagranitoids (samples GE0322 and GE0021) and the younger intrusive granitoids (samples GE0140 and GE0164). Eleven monazite analyses in sample GE0322, a felsic tonalite gneiss from the older series, cluster around a weighted mean date of 341 ± 14 Ma, which is similar with the age of the metamorphic zircon rims in the tonalite gneiss GE0011 (338 ± 5 Ma). We interpret that monazite in GE0322 formed during Variscan regional metamorphism. This is consistent with the observation that the tonalite-granodiorite series mostly carry magmatic allanite (Petrik and Broska, 1994), which may react to monazite during high-grade regional metamorphism (Bingen and others, 1996). Sample GE0011 contains no monazite, but accessory xenotime crystals with high U contents were found. Th-U-total Pb ages (weighted average 330 ± 9 Ma) indicate that this xenotime also formed during Variscan regional metamorphism. Particularly interesting is the second tonalite-gneiss sample with

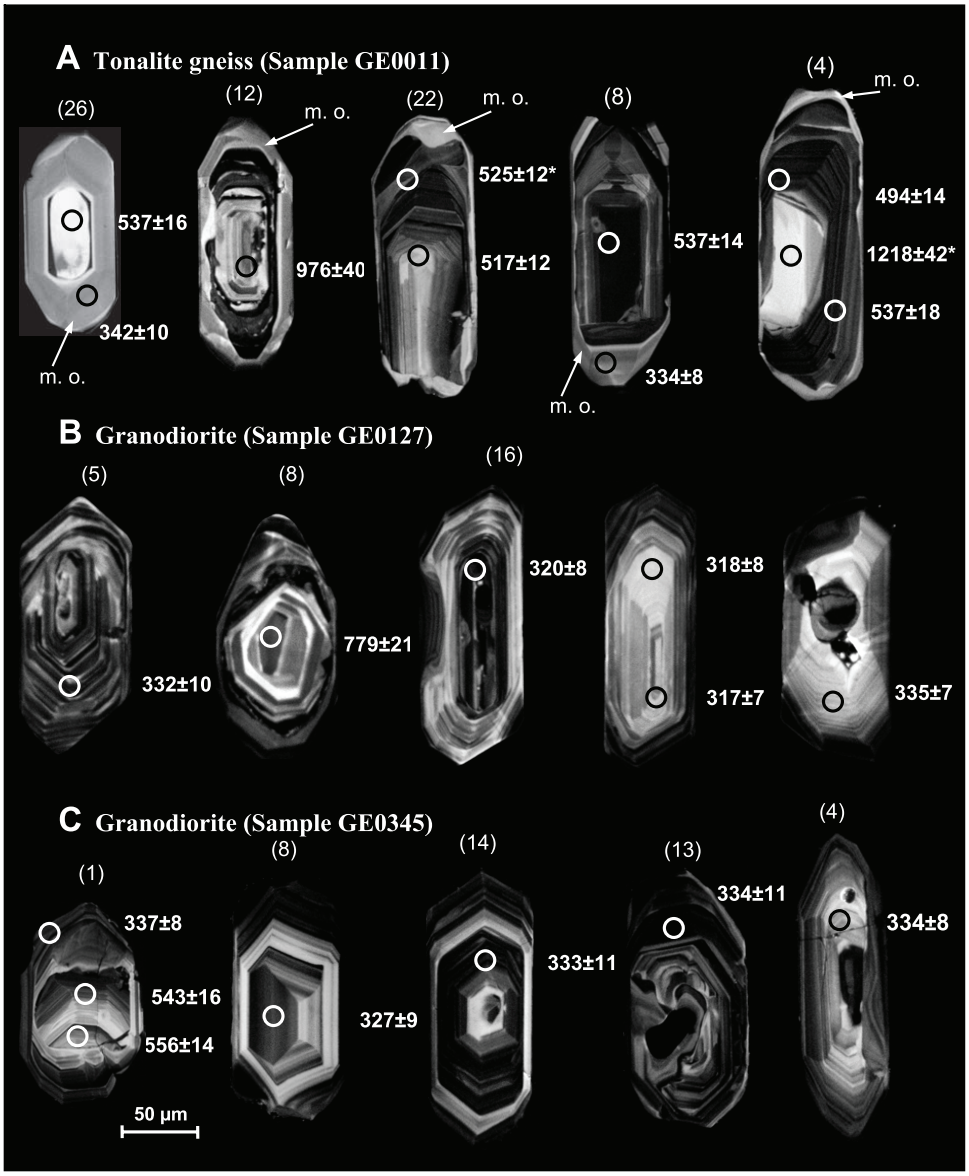

Fig. 5. Cathodoluminescence images of polished zircons from three samples of the tonalite granodiorite complex, dated by LA-ICP-MS. Shown age dates (in million years) refer to ^{238}U-^{206}Pb ages, except for numbers with star, which are ^{207}Pb-^{206}Pb ages. Errors are 2σ. Note the characteristic metamorphic overgrowths (m. o.) in the tonalite gneiss GE0011.

monazite (GE0021). A thin section of this sample contained two Variscan monazite grains, with one grain containing an older core with an age of 516 ± 36 Ma. This may be a rare example of a preserved primary igneous monazite since the age is similar to the igneous zircon age recorded in the tonalite-gneiss sample GE0011.

Monazite was found in two felsic samples from the younger tonalite-granodiorite series (GE0140 and GE0164). The two obtained weighted average ages (314 ± 19 Ma,

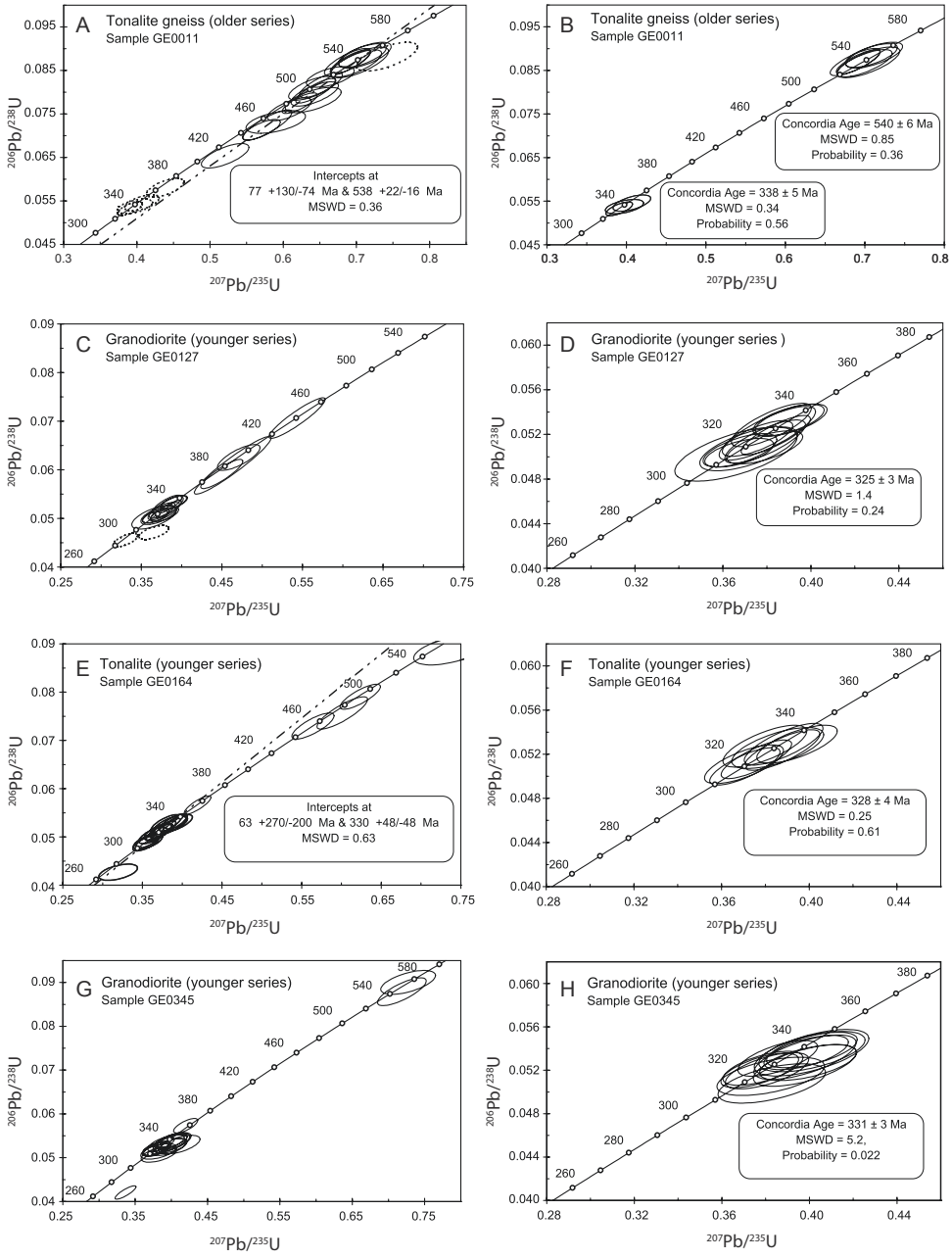

Fig. 6. U-Pb concordia diagrams illustrating the zircon dating results for samples GE0011 (A, B), GE0127 (C, D), GE0164 (E, F) and GE0345 (G, H).

332 ± 29 Ma) overlap in error with the zircon ages obtained for this series. The monazite grains are likely to be of igneous origin as the Y_2O_3 contents (1-3 wt.%) are too high for hydrothermal or low-grade metamorphic formation (Heinrich and others, 1997; Pyle and others, 2001).

TABLE 2

Results of EMP monazite dating on samples from the tonalite-granodiorite complex

Grain spot	Th wt.%	U wt.%	Pb wt.%	Th* wt.%	Age (Ma)	±	2σ
Felsic tonalite-gneiss (sample GE0322)							
m 1.1	4.552	0.122	0.070	4.947	315	±	47
m 2.1	2.725	0.318	0.061	3.761	364	±	62
m 2.2	1.867	0.259	0.041	2.712	340	±	86
m 3.1	4.989	0.250	0.094	5.804	362	±	40
m 3.2	5.177	0.256	0.091	6.011	338	±	39
m 3.3	4.436	0.138	0.077	4.885	354	±	48
m 3.4	4.993	0.132	0.078	5.421	324	±	43
m 4.1	4.944	0.265	0.080	5.804	310	±	40
m 4.2	0.368	0.198	0.009	1.007	204	±	233
m 5.1	4.624	0.183	0.088	5.223	376	±	45
m 5.2	4.717	0.133	0.079	5.149	344	±	45
					341	±	14
Tonalite-gneiss (sample GE0011); xenotime							
x 1.1	0.262	3.696	0.172	12.267	317	±	22
x 2.1	0.264	3.712	0.185	12.342	338	±	22
x 3.1	0.041	2.864	0.136	9.353	328	±	29
x 4.1	0.063	2.879	0.141	9.430	338	±	28
x 5.1	0.720	1.642	0.087	6.087	325	±	39
x 6.1	0.628	1.533	0.087	5.620	349	±	68
x 6.2	0.718	1.708	0.088	6.267	316	±	61
x 7.1	0.221	3.143	0.162	10.455	350	±	37
x 7.2	0.305	4.044	0.186	13.435	312	±	29
x 7.3	0.093	3.240	0.149	10.617	316	±	36
x 7.4	0.164	3.489	0.178	11.525	348	±	33
x 8.1	0.944	1.891	0.104	7.092	331	±	54
x 8.2	0.508	1.366	0.069	4.946	315	±	78
x 9.1	0.714	2.352	0.131	8.375	352	±	46
x 9.2	0.732	2.455	0.123	8.709	318	±	44
					330	±	9
Tonalite-gneiss (sample GE0021)							
m 1.1	5.478	0.775	0.186	8.034	516	±	36
m 1.2	4.986	0.605	0.108	6.956	348	±	42
m 2.1	4.450	0.463	0.091	5.958	340	±	49
m 2.2	4.356	0.454	0.094	5.835	362	±	50
					349	±	26
Felsic tonalite (sample GE0140)							
m1.1	4.065	0.146	0.067	4.538	331	±	46
m1.2	3.785	0.237	0.071	4.556	349	±	46
m2.1	2.143	1.876	0.119	8.240	325	±	26
m2.2	1.666	1.212	0.078	5.601	312	±	38
m3.1	0.279	2.422	0.108	8.136	299	±	26
m3.2	0.236	2.060	0.092	6.917	299	±	30
					314	±	19
Felsic quartz-diorite (sample GE0164)							
m 1.1	3.908	0.082	0.061	4.173	327	±	57
m 2.1	3.415	0.090	0.056	3.708	339	±	64
m 1.2	3.924	0.100	0.063	4.249	332	±	56
m 2.2	3.490	0.086	0.056	3.771	331	±	63
					332	±	29

Single point ages, errors and weighted average ages (95% CL) calculated according to Montel and others (1996). Sample locations: GE0322: river outcrop, Chelmosmula River, 1.1 km north of Dzirula River; GE0011: see table 1; GE0021: river outcrop, Chelmosmula River, 4.1 km north of Dzirula River; GE0140: river outcrop, Gezrula River, 4.7 km north of Dzirula River; GE0164: see table 1.

Metapelitic Paragneisses and Migmatites

Monazite is abundant in the metapelitic paragneisses and migmatites. We analyzed more than 30 grains from 8 samples with the electron microprobe (table 3, fig. 7). Most grains yielded Variscan Th-U-total Pb ages, with weighted averages scattering between 325 and 342 Ma. However, in four samples, pre-Variscan monazite was found as well. These relict monazite grains display Early Palaeozoic ages and imply that an earlier metamorphic event may have affected the metapelitic series, most likely in the Ordovician. The Early Palaeozoic monazite is normally overgrown by variably thick Variscan rims. In GE0316, Variscan monazite rims were not found, and all monazite grains in this sample appear to have formed in the Early Palaeozoic (table 3, fig. 7). Since the risk of mixing ages is lowest in this sample, we consider the weighted mean age of 439 ± 20 Ma as the best age estimate for the pre-Variscan metamorphic event.

GEOCHEMISTRY

Analytical Procedure

We analyzed 77 rocks from the Dzirula massif for major, trace, and rare earth elements. Major element and most trace element analyses were carried out by XRF techniques at Salzburg University on a Bruker instrument S4 Explorer equipped with a 4 kW Rh-anode tube. For trace elements, which were measured on pressed powder pellets, counting times and tube conditions were optimized automatically up to 4 kW and 400 s per element, respectively, to obtain a detection limit of at least 3 ppm (3σ). Typical errors (2σ) from the counting statistics were 1 to 2 ppm at low concentrations <10 ppm, 2 to 5 ppm at the 10 to 100 ppm concentration level, and better than 5 percent (relative) for higher concentrations. Major elements were determined on glass beads at reduced tube energies. Counting times were chosen in a way that the relative 2σ uncertainties were better than 1 percent for SiO_2 and Al_2O_3, and better than 5 percent for elements at the 1 to 10 weight percent concentration level.

Trace elements with low concentrations like Hf, Ta, Th, U, and the rare earth elements were determined by ICP-MS techniques at Kingston University. Typical errors (2σ) were better than 0.1 ppm. Analytical techniques are described by Jarvis and Williams (1993).

The Metapelites

The metapelites are characterized by a strongly peraluminous composition with A/CNK values between 1.3 and 2.2 (fig. 8). They have the bulk whole-rock composition of shales to graywackes. Plotted on a Sc-Th-Zr/10 diagram (not shown), they indicate a continental island arc source (Bhatia and Crook, 1986). Compared to the granitoids, they typically have higher contents of Cr and Ni and lower contents of CaO, Na_2O, and Sr. Some of the thin amphibolitic layers within the metapelites were also analyzed. These rocks display tholeiitic MORB-type compositions and thus deviate from the calc-alkaline mafic enclaves found in the metagranitoid group.

The Tonalite-Granodiorite Complex

Both the deformed (Cambrian) and undeformed (Variscan) varieties of the tonalites and granodiorites have similar whole-rock geochemistry and cannot be discriminated on a chemical basis. Both series show an extended SiO_2 variation of ~55 to 72 weight percent and A/CNK values of mostly 0.9 to 1.1, that is, features typical of I-type granite suites (Chappell and White, 1974). According to the classification of Frost and others (2001) the rocks can be described as magnesian granitoids, with a mostly calcic to calc-alkalic composition.

However, both age groups include magmas of different origins, as evidenced by the presence of high-K and medium-K variants in the K_2O vs SiO_2 diagram (fig. 8)

Table 3

Results of EMP monazite dating on metapelite samples from the Dzirula massif

Grain spot	Th wt.%	U wt.%	Pb wt.%	Th* wt.%	Age (Ma)	±	2σ
Sample GE0138							
m 1.1	4.092	0.240	0.074	4.873	338	±	43
m 1.2	3.643	0.280	0.070	4.556	345	±	46
m 2.1	1.036	0.846	0.054	3.785	321	±	56
m 3.1	0.015	2.418	0.115	7.876	328	±	27
m 4.1	0.064	2.405	0.114	7.882	326	±	27
					330	±	15
Sample GE0144							
m 1.1	4.538	0.341	0.083	5.647	331	±	52
m 1.2	4.221	0.401	0.082	5.523	332	±	53
m 2.1	4.395	0.128	0.070	4.812	325	±	60
					330	±	31
Sample GE0152							
m 1.1	4.276	0.638	0.090	6.349	318	±	38
m 1.2	4.394	0.948	0.105	7.472	316	±	32
m 1.3	4.309	0.651	0.099	6.430	346	±	37
m 1.4	4.290	0.643	0.095	6.381	333	±	37
m 1.5	4.701	0.473	0.102	6.244	365	±	38
m 1.6	4.392	0.509	0.094	6.049	349	±	40
m 1.6	4.310	0.475	0.081	5.853	312	±	41
m 2.1	5.333	0.390	0.099	6.600	334	±	36
m 4.1	4.158	0.212	0.073	4.849	339	±	49
m 5.1	4.827	0.341	0.091	5.935	345	±	40
m 6.1	4.946	0.674	0.104	7.138	328	±	34
					334	±	11
Sample GE0233							
m 1.1	3.847	1.158	0.123	7.620	362	±	31
m 1.2	3.942	1.136	0.117	7.641	344	±	31
m 1.4	3.482	0.788	0.082	6.041	305	±	39
m 1.5	3.436	0.760	0.095	5.913	360	±	39
m 3.1	3.664	0.705	0.089	5.957	335	±	39
m 3.2	3.654	0.687	0.082	5.884	311	±	40
m 6.1	4.258	0.603	0.085	6.215	308	±	38
m 6.2	4.269	0.623	0.084	6.290	300	±	37
m 7.1	3.450	1.049	0.093	6.853	305	±	34
m 7.3	3.520	1.162	0.100	7.292	308	±	32
m 8.1	4.481	0.783	0.108	7.031	344	±	33
m 8.2	4.550	0.786	0.094	7.098	299	±	33
m 8.3	4.490	0.747	0.101	6.917	329	±	34
					325	±	14

TABLE 3
(continued)

Grain spot	Th wt.%	U wt.%	Pb wt.%	Th* wt.%	Age (Ma)	±	2σ
Sample GE0316							
m 1.1	4.290	0.820	0.133	6.975	427	±	33
m 1.2	4.098	0.972	0.145	7.288	447	±	32
m 2.1	3.340	0.359	0.091	4.519	449	±	51
m 3.1	3.638	0.922	0.130	6.659	438	±	35
m 4.1	4.149	1.085	0.144	7.702	420	±	30
m 5.1	4.142	0.920	0.135	7.156	422	±	33
m 5.2	4,314	0.714	0.144	6,662	482	±	34
					439	±	20
Sample GE0151							
m 1.1	3.739	0.927	0.152	6.792	502	±	43
m 1.5	4.763	0.543	0.122	6.539	418	±	44
m 1.6	2.661	0.384	0.096	3.929	544	±	74
m 1.7	4.648	0.270	0.106	5.534	428	±	52
m 1.9	4.827	0.438	0.137	6.268	487	±	46
m 4.1	9.956	0.774	0.263	12.499	470	±	23
m 4.2	10.027	0.507	0.268	11.698	511	±	25
					482	±	32
m 1.2	4.770	0.289	0.084	5.708	330	±	51
m 1.4	4.472	0.512	0.094	6.137	343	±	47
m 1.8	3.997	0.269	0.081	4.874	370	±	60
m 2.1	4.288	0.555	0.088	6.091	325	±	48
m 2.2	4.713	0.262	0.083	5.566	334	±	52
m 3.1	4.098	0.484	0.080	5.670	314	±	51
m 4.3	3.560	0.567	0.089	5.408	370	±	54
					339	±	19
Sample GE0153							
m 1.1	3.109	0.282	0.088	4.035	484	±	52
m 1.2	3.858	0.463	0.082	5.366	342	±	39
m 2.1	3.746	0.843	0.100	6.490	346	±	32
m 2.2	4.769	0.431	0.090	6.169	327	±	34
m 3.1	5.129	0.362	0.099	6.308	351	±	33
					342	±	17

(Roberts and Clemens, 1993). Included among the older metagranitoids are fairly abundant and relatively felsic, medium-K biotite-tonalites and trondhjemites with SiO_2 contents around 70 weight percent. Among the younger granitoids high-K types are comparably more dominant, but there are also medium-K variants (fig. 8). Within the younger metagranitoids, two subgroups of high-Zr and low-Zr granitoids are distinguished. On Pearce-type Nb vs Y and Rb vs Y+Nb plots (not shown) the granitoids plot generally in the volcanic arc granite field.

TABLE 3
(continued)

Grain spot	Th wt.%	U wt.%	Pb wt.%	Th* wt.%	Age (Ma)	±	2σ
Sample GE0163							
m 3.1	2.551	0.550	0.098	4.363	502	±	48
m 3.2	3.121	0.891	0.129	6.052	476	±	35
m 3.3	3.192	1.039	0.139	6.606	472	±	32
m 4.2	3.011	0.978	0.123	6.218	445	±	34
					470	±	33
m 1.1	4.478	0.389	0.082	5.744	321	±	36
m 1.2	3.917	0.247	0.071	4.719	338	±	44
m 2.1	5.135	0.473	0.099	6.674	333	±	31
m 4.1	3.951	0.757	0.103	6.418	360	±	33
					339	±	17

Single point ages, errors and weighted average ages (95% CL) calculated according to Montel and others (1996). Sample locations: GE0138: river outcrop, Matscharula River, 3.3 km north of Shroscha; GE0144: river outcrop, Gezrula River, 4.9 km north of Dzirula River; GE0152: river outcrop, Dumala River, 4.3 km north of Dzirula River; GE0233: river outcrop, Zcheritela River, 15.5 km southeast of Dzirula River; GE0316: river outcrop, Matscharula River, 6.2 km north of Shroscha; GE0151: river outcrop, Dumala River, 4.3 km north of Dzirula River; GE0153: river outcrop, Dumala River, 4.5 km north of Dzirula River; GE0163: river outcrop, Kvirila River, 8.6 km north of Dzirula River.

Multi-element variation diagrams normalized against primitive mantle (fig. 9) show a slight depletion of the High Field Strength Elements (HFSE) when compared with the Large Ion Lithophile Elements (LILE). Negative anomalies in Ta, Nb, Sr, P and Ti are typical of volcanic arc plutons (Tarney and Jones, 1994). The rare earth element plot (fig. 9) illustrates light rare earth element (LREE) enrichment and flat profiles for the heavy rare earth elements (HREE) when normalized against chondrite (Sun and McDonough, 1989). The mean $La/Yb_{(N)}$ value for all the tonalites and granodiorites is 6.97, with early ones at 6.06 and late ones at 7.74. Most samples exhibit a negative Eu-anomaly. A few samples with low total REE contents display minor positive Eu anomalies, probably due to plagioclase accumulation.

The Pink Granites

The pink granites form a distinct group of felsic magmas characterized by high SiO_2 (71-78 wt.%), low CaO (<1 wt.%), and high alkali contents (Na_2O 3-4 wt.%, K_2O 4-6 wt.%). Using the classification of Frost and others (2001), the rocks can be described as ferroan, alkali-calcic granitoids. A/CNK ratios are close to 1.1, and straddle the I-/S-type granite boundary (fig. 8). However, the generally low P_2O_5 contents are more typical of I-type granites (Chappell, 1999).

With reference to their trace element composition, the pink granites are best classified as volcanic arc granites (Pearce and others, 1984). The multi-element variation diagram (fig. 10) shows a mean $(LILE/HFSE)_N$ ratio of ~50 and the rare earth element plot a $(LREE/HREE)_N$ ratio of ~8. The multi-element variation diagram (fig. 9) shows marked negative Nb, Ta, Sr, P and Ti anomalies. The rare earth plot shows a negative Eu-anomaly, LREE enrichment, and a flat HREE profile when normalized against chondrite. These data are similar to those from many volcanic arcs (Tarney and Jones, 1994). The results are consistent with a melting and fractionation

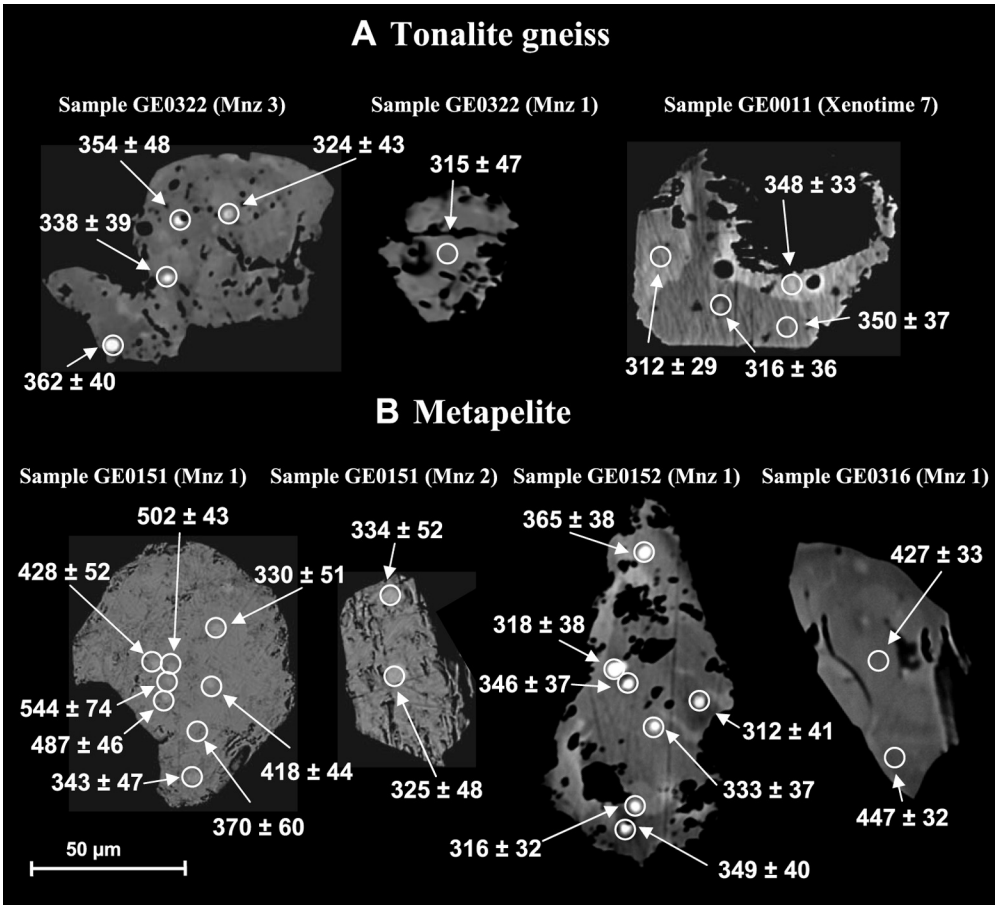

Fig. 7. Backscattered electron images of monazite and xenotime grains dated by means of the electron microprobe. (A) Variscan monazite and xenotime from tonalite gneiss. (B) Monazite from metapelite samples GE0151, GE0152 and GE0316. The grain on the left side has an older (Early Palaeozoic) core domain overgrown by a Variscan rim. The grain on the right side shows an Early Palaeozoic age in the core and at the rim. The middle two grains appear to be entirely Variscan.

scenario, which likely involves biotite- and/or hornblende-breakdown that left plagioclase and pyroxene in the residue. There is a large variation in Ba (200-1700 ppm), Zr (100-300 ppm), Y (10-50 ppm), and REEs (Ce: 40-140 ppm) contents. There is also a positive correlation between these elements and a negative one with SiO_2 (fig. 8). Sr decreases with increasing SiO_2 from *ca.* 100 ppm to *ca.* 30 ppm. These chemical trends can be best interpreted as effects of feldspar + biotite + zircon + allanite fractionation. Interestingly, there is no significant change in the magnitude of the Eu-anomaly, which may be attributed to a high fO_2 environment. The lack of CaO- and/or FeO enriched end members in the pink granite suite implies that the rocks represent restite-poor melts.

The Basic Rocks

The basic rocks of the Dzirula massif exhibit contrasting geochemical signatures. The basic meta-volcanic rocks of the Chorchana-Utslevi zone (CHUZ) have been recognized as having a N-MORB chemical signature by Zakariadze and others (2007).

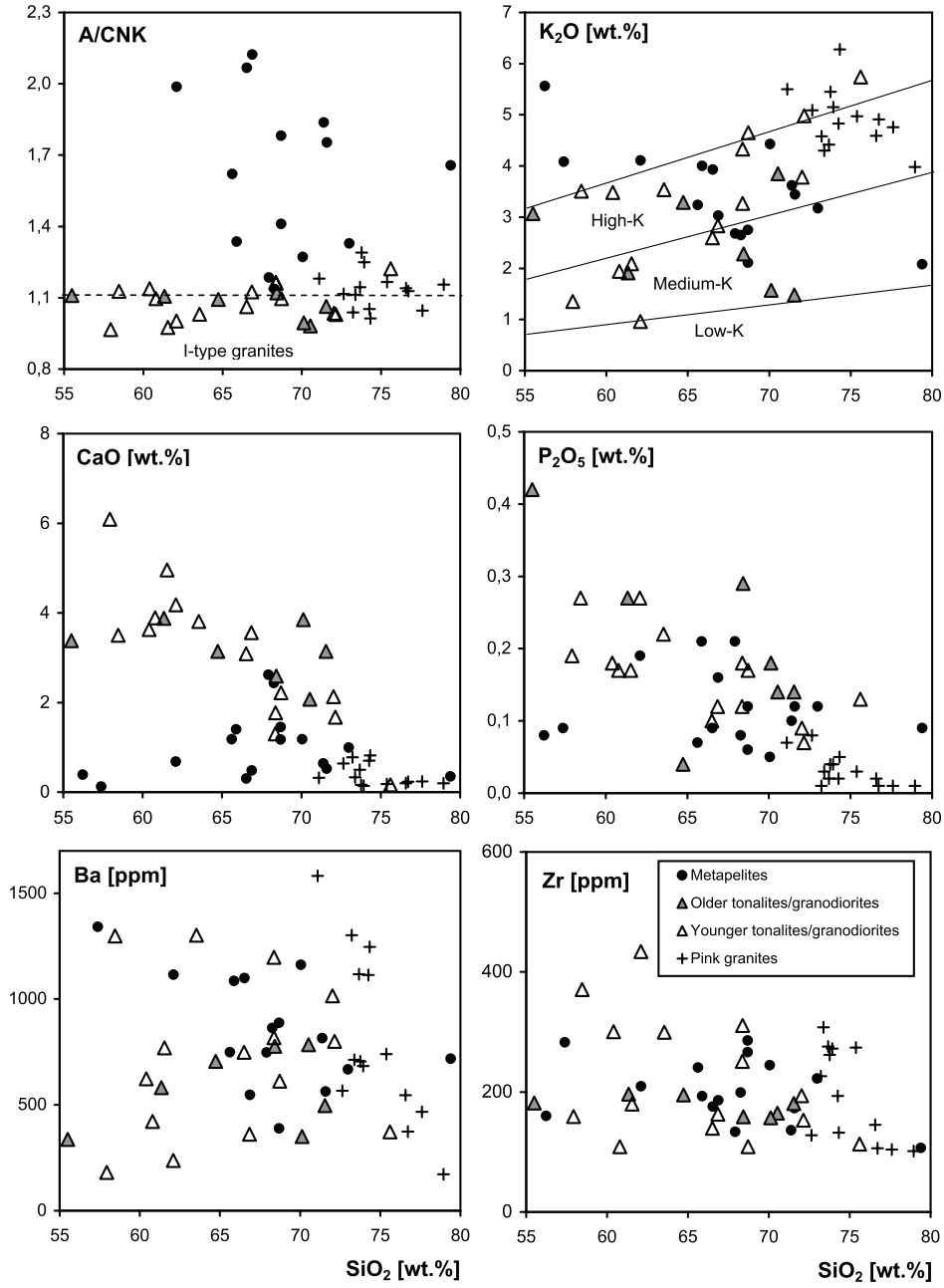

Fig. 8. Selected Harker diagrams with plots of metapelites, older and younger tonalites-granodiorites, and pink granites.

This is consistent with new analyses made during this study for this rock type (fig. 11, table 4).

The metabasic bodies mapped in the eastern part of the Dzirula massif (fig. 1) comprise mainly gabbroic-dioritic rocks with a LREE enrichment and a Th/Nb ratio

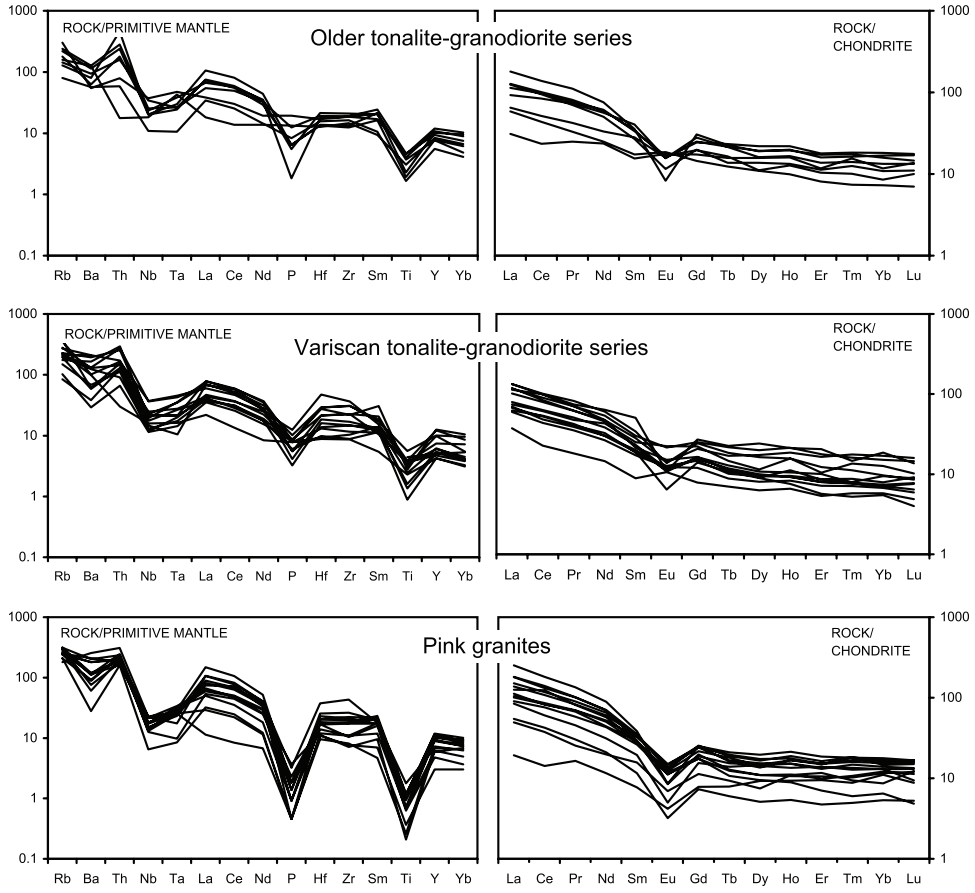

Fig. 9. Multi element and REE spider diagrams for older metagranitoids, Variscan tonalites/granodiorites and pink granites normalized versus primitive mantle and chondrite, respectively (normalizing values from Sun and McDonough, 1989).

significantly higher than MORB. The rocks appear similar to subduction related mafic magmas (Floyd and Winchester, 1975). Chemically-similar rocks occur in the western Dzirula massif near Shroscha. Figure 11 shows that most of these are LREE-enriched gabbros/basalts with high Th/Ta and Th/Nb ratios typical for magmas derived from a subduction-modified mantle source.

Finally, as briefly mentioned above, the thin metabasaltic layers within the metapelites are MORB-type with respect to their flat chondrite-normalized REE patterns and relatively low Th/Nb ratios, and they are typically depleted in the HREEs relative to the CHUZ belt metabasalts.

Hf-isotopes

Analytical Procedure

Some of the zircons from tonalite-granodiorite samples GE0011 (older group) and GE0345 (younger group) dated by LA-SF-ICP-MS (table 1) were also analyzed for their Hf isotope composition in order to derive information about their magma sources regions. Hafnium isotope measurements were performed using a Thermo-

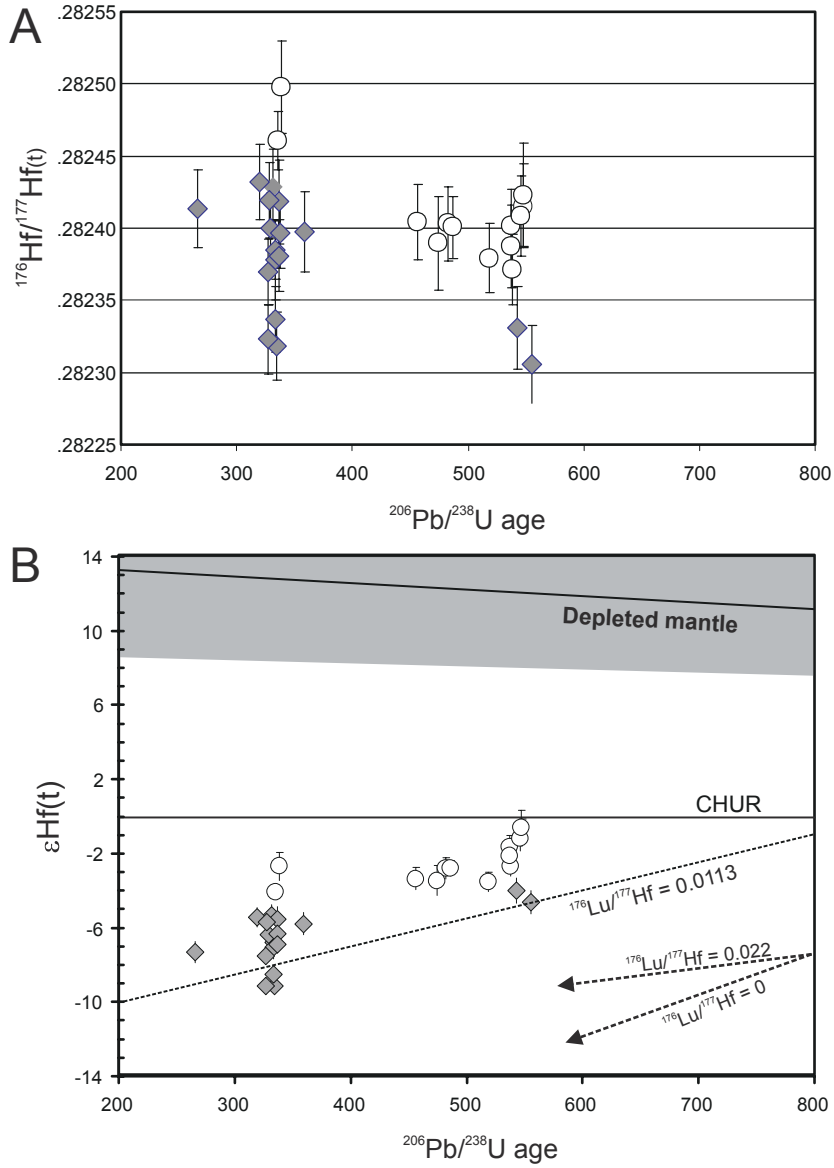

Fig. 10. $^{176}Hf/^{177}Hf(t)$ vs zircon age diagram (A) and εHf(t) vs zircon age diagram (B), showing the results of all Lu-Hf isotope spot analyses on zircons from samples GE0011 (tonalite gneiss) and GE0345 (granodiorite). CHUR: evolution of the chondritic uniform reservoir (data from Bouvier and others, 2008). Arrows show evolution trends of εHf values as a function of Lu/Hf whole rock contents.

Scientific Neptune multi-collector (MC-)SF-ICP-MS at the Institute of Geosciences (GUF), Frankfurt, coupled to the same laser system and ablation cell described earlier in the geochronology section. Data were collected in static mode (^{172}Yb, ^{173}Yb, ^{175}Lu, ^{176}Hf-Yb-Lu, ^{177}Hf, ^{178}Hf, ^{179}Hf, ^{180}Hf) during 55 seconds of laser ablation. The Lu-Hf laser spot of 40 μm diameter was commonly set directly beside or above the 30 μm U-Pb laser spot, and thus in the same zircon domain that was used for dating. More details of the analytical procedure are given in Gerdes and Zeh (2006, 2009). All

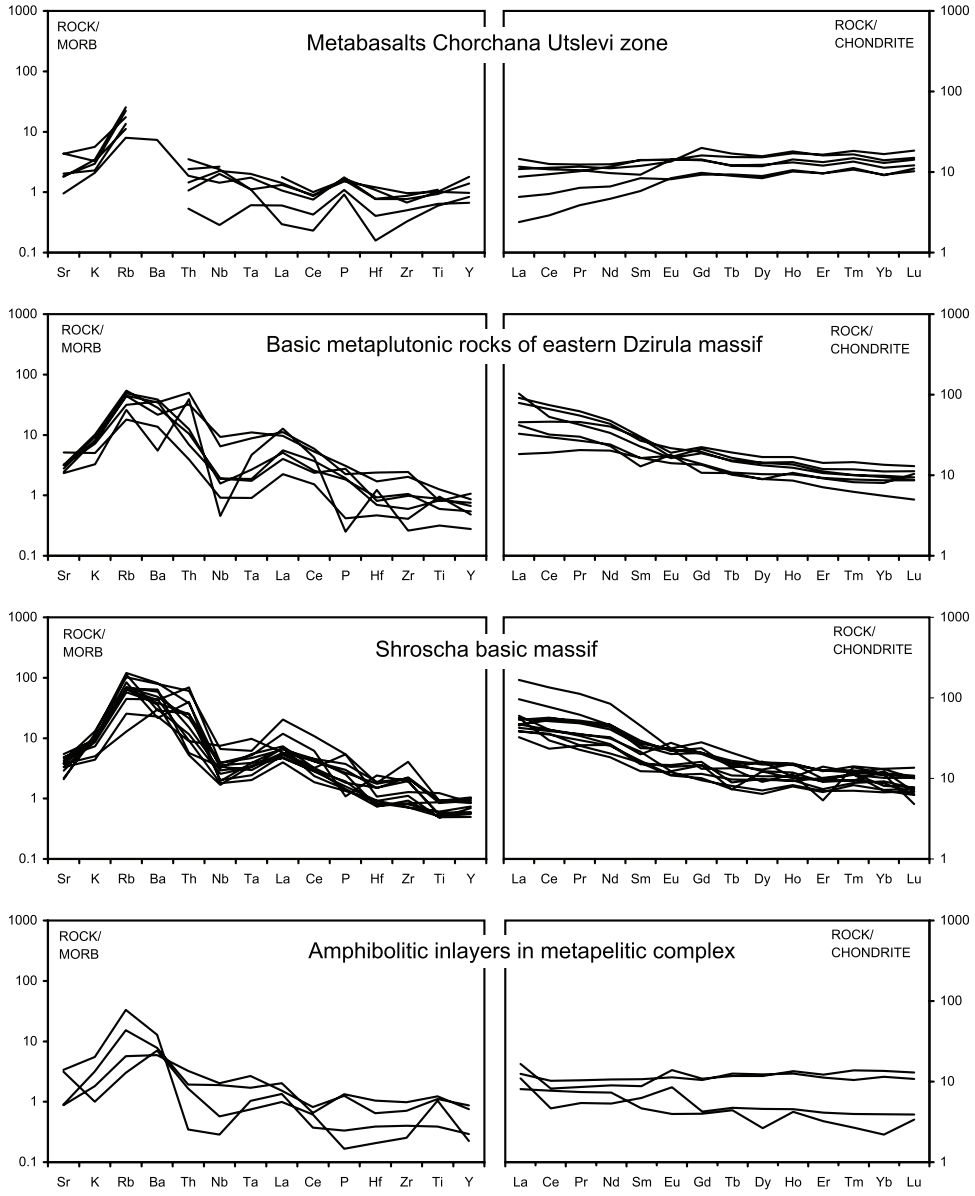

Fig. 11. MORB normalized trace element patterns and chondrite normalized REE patterns for the basic rocks from the Dzirula massif. Normalizing values are from Pearce (1983) and Sun and McDonough (1989). The CHUZ data include four analyses from Zakariadze and others (1998).

analyses were adjusted relative to the JMC 475 $^{176}Hf/^{177}Hf$ ratio of 0.282160. The external reproducibility (2 SD; $n > 50$) based on over 6 months of analyses of reference zircons 91500, GJ-1, and Plešovice ($^{176}Hf/^{177}Hf = 0.282298 \pm 0.000026$, 0.282003 ± 0.000018, and 0.282482 ± 0.000015, respectively) at GUF was about 0.005–0.009% (<1 epsilon unit). External reproducibility was the same for analyses with higher $^{176}Yb/^{177}Hf$ compared to the zircon standards (Gerdes and Zeh, 2009).

Table 4

Representative geochemical analyses of major rock types of the Dzirula massif

rock	OTG	OTG	YTG	YTG	YTG	MP	MP	PG	PG	B1	B2	B3	B4
sample	GE0343	GE0011	GE0164	GE0345	GE0127	GE0138	GE0151	GE0338	GE0182	GE0132	GE0236	GE0237	GE0221
SiO_2	61.34	68.42	62.09	63.54	68.37	65.89	68.70	73.22	77.60	50.11	49.84	47.19	51.12
TiO_2	0.90	0.59	0.70	0.74	0.53	0.74	0.77	0.14	0.04	0.98	0.96	0.63	1.80
Al_2O_3	15.51	14.71	18.87	16.89	15.22	14.65	15.69	13.32	12.66	18.38	20.37	21.3	12.83
Fe_2O_3	7.74	4.52	1.99	5.59	4.34	6.09	4.79	2.26	0.47	10.04	6.76	5.86	13.81
MnO	0.09	0.08	0.04	0.10	0.06	0.08	0.04	0.04	0.00	0.18	0.15	0.09	0.28
MgO	3.15	2.22	1.41	1.57	1.07	2.38	1.35	0.24	0.00	5.05	4.58	5.77	7.81
CaO	3.88	2.59	4.18	3.81	1.77	1.40	1.45	0.78	0.24	8.65	8.93	9.77	7.58
Na_2O	2.98	3.62	6.20	3.42	3.86	2.49	1.94	3.93	3.96	1.90	3.00	3.11	2.37
K_2O	1.91	2.28	0.96	3.54	3.27	4.00	2.75	4.58	4.76	1.97	1.97	1.16	0.38
P_2O_5	0.27	0.29	0.27	0.22	0.18	0.21	0.06	0.01	0.01	0.17	0.22	0.04	0.15
SO_3	0.23	0.02	0.28	0.06	0.03	0.01	0.01	0.01	0.01	0.08	0.17	0.05	0.04
LOI	2.75	1.01	3.88	1.29	1.88	1.97	2.88	1.04	0.42	2.93	3.09	4.99	1.87
Total	100.75	100.35	100.87	100.77	100.59	99.91	100.43	99.57	100.17	100.44	100.04	99.96	100.04
Ba	581	777	237	1302	818	1085	887	1302	467	400	537	179	82
Cr	112	52	29	32	34	111	73	6	3	80	205	206	130
Ga	22	20	25	22	26	22	19	20	18	25	18	17	17
Nb	22	12	16	15	24	18	16	10	11	7	6	b.d.l.	7
Ni	55	15	4	12	2	35	23	2	b.d.l.	11	14	81	53
Pb	14	21	15	23	35	20	23	26	22	5	14	b.d.l.	6
Rb	86	95	51	163	128	150	82	149	180	143	62	42	7
Sc	26	14	17	19	17	17	10	9	2	38	29	32	47
Sr	253	338	397	289	188	201	223	86	42	430	316	384	100
V	198	82	61	74	67	137	94	3	b.d.l.	348	182	161	442
Y	38	34	30	49	51	32	33	37	25	27	19	11	31
Zn	114	72	58	82	87	96	54	45	9	139	82	34	144
Zr	196	159	434	299	311	193	286	227	104	74	110	42	74

Table 4
(continued)

rock	OTG	OTG	YTG	YTG	YTG	MP	MP	PG	PG	B1	B2	B3	B4
sample	GE0343	GE0011	GE0164	GE0345	GE0127	GE0138	GE0151	GE0338	GE0182	GE0132	GE0236	GE0237	GE0221
Hf	5.4	3.6	13.4	8.3	7.7	5.7	6.9	5.2	3.2	2.2	2.4	1.0	1.7
Ta	1.0	1.6	1.0	1.3	1.6	1.0	0.8	0.9	0.9	0.4	0.5	0.2	0.5
Th	12.9	1.4	10.3	13.9	22.1	11.9	18.7	14.7	14.2	4.8	2.3	0.1	0.6
U	3.3	2.1	4.5	3.2	5.4	3.6	2.5	4.1	2.5	1.5	0.7	0.1	0.4
La	34.1	11.4	27.2	43.0	41.5	33.7	53.0	55.7	18.1	15.6	15.3	4.0	4.6
Ce	80.6	22.4	58.8	85.8	95.5	71.5	112.1	112.4	36.0	37.0	30.7	4.5	9.8
Pr	9.9	3.4	6.5	9.6	10.2	8.4	12.4	12.3	3.5	4.9	4.1	0.7	1.4
Nd	40.0	16.9	30.5	38.3	45.2	34.7	46.4	46.4	14.1	22.1	16.4	3.8	7.5
Sm	9.3	3.6	5.8	7.0	11.7	7.1	8.1	7.8	3.6	4.9	3.0	1.4	2.5
Eu	1.4	1.5	1.9	1.9	0.9	1.7	1.6	1.2	0.6	1.1	1.6	0.7	1.0
Gd	8.5	5.3	6.8	7.7	8.3	8.7	7.5	7.4	3.4	4.5	3.3	1.3	3.2
Tb	1.2	0.9	0.8	1.3	1.3	1.1	0.9	1.0	0.5	0.6	0.6	0.3	0.7
Dy	6.1	6.0	4.4	7.6	9.2	4.9	5.5	5.9	2.8	4.1	3.4	1.7	4.7
Ho	1.3	1.2	1.2	1.6	1.6	0.9	1.1	1.2	0.8	0.8	0.8	0.3	1.0
Er	3.4	2.9	2.6	4.4	5.1	2.7	3.2	3.4	2.9	2.3	2.3	1.0	2.8
Tm	0.5	0.6	0.5	0.6	0.5	0.4	0.5	0.5	0.3	0.4	0.3	0.1	0.4
Yb	3.3	2.9	3.1	3.7	4.6	2.2	3.0	3.2	2.2	2.0	2.0	1.0	2.8
Lu	0.5	0.5	0.4	0.6	0.5	0.4	0.4	0.5	0.5	0.3	0.4	0.1	0.4

OTG: older tonalite-granodiorite series (sample locations: GE0011: see table 1; GE0322: see table 2), YTG: younger tonalite-granodiorite series (GE0127; GE0164; GE0345: see table 1), MP: metapelites GE0151; GE0163: see table 3), PG: pink granites (GE0182: road cut, Utslevi; GE0326: river outcrop, Chelmosmula River, 0.4 km north of Dzirula River); B1–4: various basic rocks, 1: Shroscha gabbro (GE0132: river outcrop, Matscharula River, 0.3 km north of Shroscha), 2: metadiorite from Chorchana-Utslevi complex (GE0236: road cut, main road from Ali to Dschwari, 2.1 km south of Utslevi), 3: metabasalt, Chorchana-Utslevi complex (GE0237: road cut, main road from Ali to Dschwari, 1.9 km south of Utslevi), 4: amphibolitic inlayer in metapelite (GE0221: river outcrop, Chelmosmula River, 4.1 km north of Dzirula River).

Hf Isotope Data

The results for the Lu-Hf isotope analyses are presented in table 5 and figure 10. Seventeen Hf isotope spot analyses were performed on 12 zircon grains from sample GE0345 and 13 analyses on 12 grains from sample GE0011. Overall, the initial $^{176}Hf/^{177}Hf_{ini}$ varies from 0.28231 to 0.28250, corresponding to εHf_t values of −0.6 to −9.1.

GE0011 zircon grains show a very homogeneous $^{176}Hf/^{177}Hf_{ini}$ of 0.28240 ±0.00003, which is close to the reproducibility of the method (~1 epsilon unit). Only the younger rim domains yield slightly more radiogenic values ($^{176}Hf/^{177}Hf_{ini}$ = 0.28248 ± 0.00005), suggesting incorporation of additional radiogenic Hf in the zircon rims during Variscan migmatization. The mean εHf_t of −1.6 ± 1.1 for GE0011 grains is consistent with a crustal origin for the older granitoids, for example, partial melting of a relatively homogenous, basic to intermediate lower crustal source with a Mesoproterozoic crustal residence time (depleted mantle Hf model age). The data do not provide any evidence for the involvement of a juvenile Cadomian mantle source.

The Variscan zircon grains from sample GE0345 have $^{176}Hf/^{177}Hf_{ini}$ values of 0.28239 ± 0.00007, which correspond to crustal εHf_t values of −4.0 to −9.1. The relatively large spread of the εHf_t values may reflect a heterogeneous crustal source, suggesting that there was little to no isotopic equilibration in the magma, even on a small scale. The two analyzed Neoproterozoic/Cadomian zircon cores have similar $^{176}Hf/^{177}Hf_{ini}$ values of 0.28231 and 0.28233 and their εHf_t values are close to those of the magmatic zircons from GE0345. It is feasible that the older granitoid series served as an important magma source for the Variscan intrusions.

DISCUSSION

New Constraints on the Evolution of the Dzirula Massif

The new data presented here show that the Dzirula massif constitutes a Variscan LP-HT metamorphic terrain. The LP-HT metamorphic style is demonstrated by the anatectic cordierite- and sillimanite-bearing metapelitic rocks that are widely distributed throughout the massif. Monazite analyses and Th-U-total Pb dates from a large number of these metapelites document monazite growth at *circa* 330 to 340 Ma, interpreted as the age of LP-HT metamorphism. It is unlikely that the monazite ages from the Dzirula massif could date a younger phase of retrogression of the LP-HT rocks, as the high yttrium contents of the monazites of up to 3 weight percent are consistent with a high-T origin (Heinrich and others, 1997; Pyle and others, 2001).

We did not undertake detailed thermobarometric studies of the metapelites due to the lack of garnet and fresh cordierite. In most of our samples, cordierite was altered to pinite and garnet was absent. However, from the petrographic observation that biotite breakdown has occurred and leucosomes have formed, a temperature estimate of ≥750 °C appears realistic. The general scarcity of garnet suggests that pressures were probably not above 0.4 to 0.5 GPa (Spear and others, 1999).

The older parts of the tonalite-granodiorite complex must have experienced the Variscan LP-HT metamorphism along with the cordierite bearing metapelites. Evidence for this comes from the presence of Variscan-age metamorphic zircon rims in the older granitoids. Not only do the zircon grains display metamorphic rims dated at 338 ± 5 Ma, but also monazite and xenotime were found to be newly formed Variscan phases.

The zircon age data show that the Dzirula massif also contains Variscan tonalitic-granodioritic plutonism dated between 331 and 325 Ma. These are similar in age to LP-HT regional metamorphism in the massif. Geochemical data indicate that the Variscan tonalitic-granodioritic magmas were derived from lower crustal I-type sources. It is thus likely that the mid-Carboniferous tonalitic-granodioritic plutonic activity

TABLE 5

Hf isotope data for zircons from samples GE0011 and GE0345 (sample locations see table 1)

Grain spot	$^{176}Yb/^{177}Hf$ (a)	±2σ	$^{176}Lu/^{177}Hf$ (a)	±2σ	$^{178}Hf/^{177}Hf$	$^{180}Hf/^{177}Hf$	Sig_{Hf} (b)	$^{176}Hf/^{177}Hf$	±2σ (c)	$^{176}Hf/^{177}Hf_{(t)}$	εHf(t) (d)	± 2σ	T_{DM2} (e)	age [e] [Ma]	±2σ
Granodiorite (sample GE0345)															
1.1	0.0242	32	0.00081	9	1.46729	1.88662	9	0.282339	29	0.282331	-4.0	0.7	1.58	543	17
1.2	0.0148	12	0.00052	3	1.46726	1.88667	7	0.282311	27	0.282306	-4.6	0.6	1.62	556	15
1.3	0.0357	33	0.00118	9	1.46723	1.88659	10	0.282388	25	0.282381	-6.8	0.5	1.56	337	9
2.1	0.0682	57	0.00206	13	1.46724	1.88655	8	0.282409	24	0.282396	-6.2	0.5	1.53	337	10
3.1	0.0300	26	0.00099	7	1.46731	1.88665	6	0.282425	26	0.282419	-5.6	0.6	1.49	328	9
4.1	0.0440	38	0.00145	9	1.46736	1.88673	8	0.282346	23	0.282337	-8.4	0.4	1.65	333	9
5.1	0.0441	38	0.00144	10	1.46733	1.88643	8	0.282407	28	0.282398	-5.7	0.6	1.52	359	9
7.1	0.0432	36	0.00146	10	1.46728	1.88670	7	0.282409	25	0.282400	-6.3	0.5	1.53	330	10
10.1	0.0152	24	0.00048	7	1.46732	1.88675	6	0.282435	26	0.282432	-5.4	0.5	1.47	319	10
11.1	0.0313	66	0.00097	19	1.46720	1.88661	8	0.282329	24	0.282323	-9.1	0.5	1.68	327	9
11.2	0.0452	85	0.00141	25	1.46715	1.88655	8	0.282378	23	0.282369	-7.4	0.4	1.59	327	9
12.1	0.0382	52	0.00127	18	1.46726	1.88674	8	0.282420	27	0.282413	-7.2	0.6	1.53	266	8
12.2	0.0358	35	0.00121	10	1.46724	1.88664	8	0.282426	29	0.282418	-5.5	0.7	1.49	337	12
13.1	0.0441	40	0.00138	10	1.46732	1.88657	7	0.282327	24	0.282318	-9.1	0.5	1.68	334	11
14.1	0.0559	61	0.00198	19	1.46726	1.88671	9	0.282397	20	0.282385	-6.7	0.3	1.56	333	11
14.2	0.0363	45	0.00122	12	1.46725	1.88628	8	0.282385	28	0.282378	-7.0	0.6	1.57	333	11
22.1	0.0520	45	0.00158	11	1.46719	1.88659	7	0.282438	26	0.282428	-5.2	0.6	1.47	331	9
Tonalite-gneiss (sample GE0011)															
4.1	0.0144	14	0.00048	4	1.46720	1.88670	8	0.282392	29	0.282387	-2.1	0.7	1.47	538	19
5.1	0.0416	58	0.00130	14	1.46722	1.88677	7	0.282436	36	0.282423	-0.6	1.0	1.40	547	16
8.1	0.0498	53	0.00162	14	1.46733	1.88656	8	0.282388	25	0.282371	-2.6	0.6	1.50	538	15
8.2	0.0101	11	0.00037	4	1.46729	1.88667	7	0.282463	20	0.282461	-4.0	0.3	1.41	335	9
9.1	0.0296	27	0.00101	8	1.46728	1.88665	7	0.282413	26	0.282404	-3.3	0.6	1.47	456	14
10.1	0.0290	25	0.00097	6	1.46726	1.88662	7	0.282418	28	0.282409	-1.1	0.7	1.42	546	18
13.1	0.0487	45	0.00159	11	1.46731	1.88661	6	0.282415	21	0.282401	-2.8	0.4	1.46	486	16
14.1	0.0204	19	0.00071	5	1.46739	1.88690	5	0.282502	32	0.282498	-2.6	0.8	1.33	338	9

TABLE 5
(continued)

Grain spot	$^{176}Yb/^{177}Hf$ (a)	±2σ	$^{176}Lu/^{177}Hf$ (a)	±2σ	$^{178}Hf/^{177}Hf$	$^{180}Hf/^{177}Hf$	Sig_{Hf} (b)	$^{176}Hf/^{177}Hf$	±2σ (c)	$^{176}Hf/^{177}Hf_{(t)}$	εHf(t) (d)	±2σ	T_{DM2} (e)	age [e] [Ma]	±2σ
Tonalite-gneiss (sample GE0011)															
1.1	0.0242	32	0.00081	9	1.46729	1.88662	9	0.282339	29	0.282331	-4.0	0.7	1.58	543	17
15.1	0.0334	34	0.00107	9	1.46767	1.88697	8	0.282399	32	0.282390	-3.4	0.8	1.49	474	14
19.1	0.0496	49	0.00163	14	1.46734	1.88660	6	0.282418	26	0.282403	-2.8	0.6	1.46	482	13
21.1	0.0496	49	0.00163	14	1.46734	1.88660	6	0.282418	26	0.282401	-1.6	0.6	1.44	537	17
22.1	0.0246	25	0.00090	8	1.46722	1.88683	7	0.282368	24	0.282359	-3.5	0.5	1.53	519	13
25.1	0.0271	25	0.00101	7	1.46736	1.88673	8	0.282426	29	0.282416	-0.8	0.7	1.41	548	15
Standards															
JMC (50ppb) (n=8)					1.46716	1.88662	14	0.282155	8						
91500	0.0098	7	0.00035	1	1.46725	1.88667	7	0.282310	15	0.282303	6.8	0.5	1.41	1064	4

(a) $^{176}Yb/^{177}Hf = (^{176}Yb/^{173}Yb)_{true}(^{173}Yb/^{177}Hf)_{measx}(M(^{173}Yb)/M(^{177}Hf))b(Hf)$, $b(Hf) = \ln(^{179}Hf/^{177}Hf_{true}/^{179}Hf/^{177}Hf_{measured})/\ln(M(^{179}Hf)/M(^{177}Hf))$, M = mass of respective isotope. The $^{176}Lu/^{177}Hf$ were calculated in a similar way by using the $^{175}Lu/^{177}Hf$ and b(Yb). Quoted uncertainties (absolute) relate to the last quoted figure. The effect of the inter-element fractionation on the Lu/Hf was estimated to be about 6% or less based on analyses of the 91500 zircon.

(b) Mean Hf signal in volt.

(c) Uncertainties are quadratic additions of the within-run precision and the daily reproducibility of the 40ppb-JMC475 solution. Uncertainty for the JMC475 standard is 2SD (2 standard deviation).

(d) Initial $^{176}Hf/^{177}Hf$ and εHf calculated using the apparent U-Pb age determined by LA-ICP-MS dating (see last two rows), and the CHUR parameters: $^{176}Lu/^{177}Hf = 0.0336$, and $^{176}Hf/^{177}Hf = 0.282785$ (Bouvier and others, 2008).

(e) Two stage model age in billion years using the measured $^{176}Lu/^{177}Hf$ of each spot (first stage = age of zircon), a value of 0.0113 for the average continental crust (second stage), and a depleted mantle $^{176}Lu/^{177}Hf$ and $^{176}Hf/^{177}Hf$ of 0.0384 and 0.28325, respectively (see Gerdes and Zeh, 2006 for details and references).

played a significant role in the development of a LP-HT metamorphic regime in the Dzirula massif by transporting heat into the middle and upper crust.

The basic rocks exposed near Shroscha (fig. 1) have not yet been dated. Since these rocks lack an LP-HT overprint, they should be Variscan in age or younger and are considered part of the magmatic cause of the LP-HT metamorphism. Basic melts of this kind may have effectively transported mantle heat into the crust. We do not agree with Zakariadze and others (2007) who argued that these rocks are part of a Late Proterozoic to Cambrian island arc. The observation that some of these metabasites from Shroscha were intruded by late Variscan pink granites suggest an emplacement age of around 330 Ma, and a broadly synchronous origin with the younger tonalites-granodiorites.

The metabasic bodies mapped in the eastern Dzirula massif (fig. 1) appear to have a different origin due to evidence for a metamorphic overprint. Therefore, the protoliths to these rocks are likely pre-Variscan. Combining the Shroscha metabasite complex and these metabasic bodies in the east as one co-genetic group of volcanic arc rocks (Zakariadze and others, 2007) is therefore not viable, in our opinion. It is, however, possible that the metabasite bodies of the eastern Dzirula massif are Cadomian rocks, as proposed by Zakariadze and others (2007), although this idea would need further testing through precise geochonological data.

The pink granites, which are near-minimum I-type melts, show sharp and discordant intrusive contacts against the LP-HT metasediments and the younger metagranitoids. They should thus represent a magmatic event younger than the Variscan regional metamorphism. The mica K-Ar age of 321 ± 6 Ma (Dudauri and others, 1990) suggests that they are a late-stage part of the Variscan event. This may indicate that the high-heat flow regime was already waning during pink granite emplacement. Renewed melt production in the lower crust could be related to post-orogenic crustal uplift processes and decompression melting.

The pre-Variscan evolution of the Dzirula basement is difficult to reconstruct due to the strong Variscan metamorphic overprint. From the zircon age data, there is evidence for a significant magmatic event in the early Cambrian, which may have resulted in the emplacement of the older generation of granitoids. The age data for sample GE0011 provide a reliable formation age of 540 ± 6 Ma for the protolithic plutonic rock. Although only one sample of the older granitoids has been directly dated, a widespread Early Palaeozoic igneous event is indirectly indicated by inherited Early Palaeozoic zircon cores present in the younger Variscan granitoids. Hf isotope data for sample GE0011 imply that remelting of older crust may have played a more important role in the petrogenesis of the older Dzirula plutons than melting of juvenile mantle. This would, for the Cambrian period, favor a continental arc or continental rift setting rather than an island arc setting, as proposed by Zakariadze and others (2007).

If the MORB type rocks of the Chorchana-Utslevi-belt (CHUZ) are also Cambrian, as suggested by some authors (Gamkrelidze and Shengelia, 2001), this may provide evidence for a period of lithospheric extension and rifting at that time that led to melting in the subcontinental mantle and the lower crust of pre-existing continental lithosphere. However, since the CHUZ-belt is a tectonic sliver within the Dzirula massif, it is not certain whether it was proximal to the metagranitoid complex in the Cambrian. It could also have been positioned in a completely different place and brought into contact with the rest of the Dzirula massif during the Variscan period.

The pre-Variscan history of the Dzirula massif is also documented by the fairly abundant Early Palaeozoic monazite relics in the metapelites. The most probable interpretation is that these formed during an Early Palaeozoic (Ordovician) phase of regional metamorphism. We cannot quantify this metamorphic event since the samples

that contain old monazite do not contain phases suitable for thermobarometric estimation. The earlier paragenesis was apparently almost completely wiped out by the Variscan LP-HT metamorphism. Yttrium contents measured in the inherited monazite grains are intermediate (~2 wt.%). This indicates at least amphibolite facies temperatures. However, the degree of metamorphism may have as well been higher, since high-grade rocks often have yttrium-undersaturated monazite, due to Y partitioning into the garnet (Pyle and others, 2001; Finger and Krenn, 2007).

Data from the Greater Caucasus

There are abundant age data from the Greater Caucasus terrane to the north of the Dzirula massif that are consistent with those from the Dzirula massif. The Main Range zone of the Greater Caucasus terrane is divided into the Pass sub-zone and the Elbrus sub-zone. Two metamorphic events are recorded within the Pass subzone. The first of these, a Barrovian-type event, is dated by U-Pb zircon techniques at ~500 Ma (Hanel and others, 1993b). The second metamorphic event was of a LP/HT type. LP/HT metamorphism was Variscan in age as documented by a U-Pb zircon age of 320 ± 14 Ma (Bibikova and others, 1991) derived from syn-metamorphic quartz-diorite plutons and a Rb-Sr whole rock isochron of 316 ± 27 Ma (Ghukasiayn and Somin, 1995) derived from amphibolite facies meta-pelites. Within the Gvandra unit, staurolite is locally rimmed by cordierite. Elsewhere, staurolite is replaced by a cordierite-spinel symplectite. All these textures are consistent with LP-HT Variscan regional metamorphism. In addition, syn-metamorphic plutons with early and late Hercynian ages cut the Buulgen complex (Gamkrelidze and others, 2002).

In the Elbrus sub-zone, the basement complex is made up of meta-gabbros, biotite-bearing meta-tonalites with an arc-type TTG chemistry, and meta-pelites with evidence for partial melting (Somin and others, 2006). A SHRIMP U-Pb zircon age of 333 ± 5 Ma constrains the age of the metatonalites (Somin and others, 2006). These rocks are compositionally similar to those in the Dzirula massif and have, within error, the same age. The basement rocks show a polymetamorphic history with the highest grade metamorphism at upper amphibolite to granulite facies. Pelitic units carry the assemblage sillimanite-biotite-spinel-biotite+/−cordierite. Migmatites are widespread and may represent incomplete melt extraction following biotite fluid-absent melting. Amphibolitic units contain the assemblage hornblende-clinopyroxene-plagioclase with rare hypersthene. Somin and others (2006) report SHRIMP zircon U-Pb ages from the Elbrus zone of 305 ± 8 Ma and 307 ± 3 Ma for deformed granites and migmatites respectively. For the Adil-su and Sofiya Rivers Somin and others (2007) report SHRIMP U-Pb ages for zircon rims of 322 and 310 Ma. These data suggest that peak low pressure, high temperature metamorphism may have continued for longer in the Greater Caucasus than in the Dzirula massif.

To the west of Georgia, in the along strike continuation of the Black Sea–Central Transcaucasian Terrane, Topuz and others (2007, 2010) report data that can be compared to ours. Topuz and others (2010) date emplacement of biotite-hornblende granites mineralogically and chemically identical to those in the Dzirula massif at 320 ± 4 and 324 ± 6 Ma. Topuz and others (2007) date metamorphic cooling ages after high grade metamorphism of between 323 and 337 Ma. These ages are within error of the data presented here.

According to our petrographic and geochronological data, the Greater Caucasian Terrane and the Dzirula massif seem to have experienced a very similar geological evolution involving a combination of Cambrian-Ordovician and Variscan metamorphic/magmatic events. The Devonian Dizi Series, considered as a possible oceanic suture between the Greater Caucasus Terrane and the Black Sea–Central Transcaucasian Terrane (fig. 1), may therefore not be a major suture but instead represent just an intracontinental basin or small oceanic rift. It is unlikely to be the main Variscan suture

(Rheiic/Prototethys). This is more likely to be the suture along the northern margin of the Greater Caucasus terrane along which it sutured to the Scythian Platform. This suture is marked by eclogite-bearing blueschists metamorphosed at 1.6 ± 0.2 GPa and 600 ± 40 °C (Perchuk and Philippot, 1997) with Sm-Nd and Lu-Hf garnet ages that indicate peak metamorphism at between 310 and 330 Ma (Philippot and others, 2001). These eclogites and blueschists of the northern Caucasus are certainly potential candidates for the Rheiic/Proterotethys suture, although, like the Rhenohercynian Zone in the European Variscides, they may also represent a rift basin inboard of the Laurussian margin (von Raumer and Stampfli, 2008). Our data from the Dzirula massif do not allow any inferences on that issue.

Comparison with the Central European Variscides

Evidence for a mid-Carboniferous phase of LP-HT regional metamorphism in the Dzirula massif creates a, hitherto unreported, connection to the central and western European sections of the Variscan orogen that are characterized by Carboniferous LP-HT regional metamorphism (Zwart and Dornsiepen, 1980; O'Brien, 2000; Tropper and others, 2006). Some of the migmatitic Crd-paragneisses, and some of the anatectic (metablastic) metagranitoids of the Dzirula massif are indistinguishable from LP-HT rocks found in the Bavarian Zone of the Bohemian massif (Finger and others, 2007) or the Black Forest (Mehnert, 1968). In both localities, we find the association of LP-HT metamorphism and intense coeval granitic plutonism (Siebel and others, 2008).

Much debate has revolved around the source of heat that facilitated widespread Variscan LP-HT metamorphism. Thermal models include: subduction zone melting, slab break off, lithospheric delamination, lithospheric extension, ascent of mantle plume, thickening of a radiogenic continental crust, heat advection into the lower crust by mantle-derived magmas, convective removal of a thickened thermal boundary layer and emplacement into the upper crust of HT/HP rocks previously deeply buried into the mantle (O'Brien, 2000; Henk and others, 2000; Schulmann and others, 2005; Schaltegger and Brack, 2007). No consensus has been reached regarding the cause of Variscan metamorphism, and it appears too early to fully understand the significance of the remarkable synchroneity of low-P metamorphism and plutonism along the entire >2000 km-long belt. However, knowing that this tectonothermal regime extends also into the Caucasus and thus over the entire length of the Variscan orogen may help in developing a unified interpretation. We note however, that there is no evidence in the Caucasian terrane, including the Dzirula massif, of the HP-HT granulitic rocks, that are common in the Bohemian massif in central Europe (O'Brien, 2000). This might imply that LP-HT metamorphism is not causally connected to the HP-HT precursor regime, as has been suggested for the Central European Variscides (O'Brien, 2000).

The record of Cambrian tonalitic-granodioritic plutonism and evidence for an early Palaeozoic (Ordovician) metamorphic event in the Dzirula massif constitutes further coincidences with the central European Variscides. Both features are well known from the Amorican terranes of Central Europe (Zulauf, 1997; Timmermann and others, 2006; Dörr and Zulauf, 2010). As in the European Variscides, these events appear best explained in terms of a (late) Cadomian subduction setting followed by an Early Palaeozoic break-up of the northern Gondwana margin. Ophiolite remnants in the Variscan belt are commonly viewed as ocean floor of the coeval rift basins (for example, Finger and Von Quadt, 1995), and a comparable interpretation may be true for the Chorchana-Utslevi zone in the Dzirula massif.

In agreement with the global plate tectonic model of Stampfli and Borel (2002), we consider both the Greater Caucasus and the Black Sea–Central Transcaucasian terranes to be individual Hunic ribbon continents, which detached from the African sector of northern Gondwana in Silurian times, and accreted to the Laurasian margin

during the Variscan orogeny. Since these Hunic microcontinents represent the former Cadomian/Early Palaeozoic active margin of Gondwana, rock types and pre-Variscan orogenic imprints are necessarily similar over its whole lateral extension. This explains why the Variscan crust of the Caucasus has many features in common with the European Variscides.

By analogy with the European situation (Franke, 2000; Friedl and others, 2000; Winchester and others, 2002; von Raumer and others, 2003), parts of the Skythian platform may represent Avalonian type crust that had been accreted to the Baltic Shield during the Early Palaeozoic. This could be an interesting research target for future studies.

CONCLUSIONS

New geochemical data, together with new LA-ICP-MS zircon and electron microprobe monazite dates, are described from the Dzirula massif in the Lesser Caucasus, central Georgia. This massif is the largest basement exposure of the Variscan Black Sea-Central Transcaucasian terrane. The Dzirula massif comprises four key units:

1. Deformed tonalite-granodiorite gneisses with U-Pb zircon ages of ~540 Ma (crystallization age) and 338 Ma (metamorphic overprint).
2. LP-HT cordierite-biotite-sillimanite migmatites and paragneisses that appear to be the result of biotite fluid-absent melting. Zircon and monazite geochronology date this metamorphism at *ca.* 330 to 340 Ma. Some paragneisses contain relict Early Palaeozoic monazite that may be related to a previous thermal event.
3. Unfoliated calc-alkaline to high-K, I-type tonalites, granodiorites, diorites, and gabbros are intrusive into the gneisses and migmatites. Zircon and monazite dates of *ca.* 330 Ma suggest that these are Variscan in age and may represent the heat source that drove the LP-HT metamorphism.
4. High-K peraluminous granites, that are intrusive into all other units, have argon ages of 321 ± 7 Ma and seal the Variscan architecture.

Geochronological, petrographic, and geochemical data from the Greater Caucasus are similar to results from the Dzirula massif. The massif can thus be used as a proxy to model the evolution of the Caucasian Variscides. Like the Amorican terranes of Variscan Europe, the Caucasian Variscides belong mainly to the Hunic superterrane (Stampfli and Borel, 2002), which represents the detached Cadomian/early Palaeozoic active margin of Gondwana and accreted to Laurussia during the early Carboniferous. The I-type (TTG) character of Variscan plutonism in the Caucasus may hint to supra-subduction zone processes related to northward subduction of the Palaeotethys.

ACKNOWLEDGMENTS

We would like to thank reviewers G. Dumond and G. Stampfli, who provided several useful suggestions and comments. Discussions with J. von Raumer were helpful as well. E. Krenn is thanked for analytical assistance on the electron microprobe. We acknowledge an INTAS grant 2001-242, and support through FWF project P 18077.

REFERENCES

Adamia, Sh., Belov, A., Kekelia, M. A., and Shavishvili, I. D, 1987, Paleozoic tectonic development of the Caucasus and Turkey (Geotraverse C), *in* Flügel, H. W., Sassi, F. P., and Grecula, P., editors, Pre-Variscan and Variscan Events in the Alpine-Mediterranean Mountain Belts: Mineralia Slovaca—Monography, Alfa Bratislava, p. 23–50.

Bagheri, S., and Stampfli, G. M., 2008, The Anarak, Jandaq and Posht-e-Badam metamorphic complexes in central Iran: New geological data, relationships and tectonic implications: Tectonophysics, v. 451, n. 1–4, p. 123–155, doi:10.1016/j.tecto.2007.11.047.

Barbarin, B., 1999, A review of the relationships between granitoid types, their origins and their geodynamic environments: Lithos, v. 46, n. 3, p. 605–626, doi:10.1016/S0024-4937(98)00085-1.

Barnitsky, V. N., Dudauri, O. Z., and Stepanyuk, L. M., 1990, Geochronology of Phanerozoic granites from folded areas of Eastern Europe: Fifth working meeting Isotopes in nature, Leipzig, Central Institute of Isotopes and Radiation Research, p. 1–10.

Bhatia, M. R., and Crook, K. A. W., 1986, Trace element characteristics of graywackes and tectonic setting discrimination of sedimentary basins: Contributions to Mineralogy and Petrology, v. 92, n. 2, p. 181–193, doi:10.1007/BF00375292.

Bibikova, E. V., Somin, M. L. and Krasivskaya, I. S., 1991, U-Pb Age of Orthogneisses in the Main Caucasus Range: Izvestija Akademii Nauk SSSR, Serija Geologiceskaja, v. 9, p. 23–34.

Bingen, B., Demaiffe, D., and Hertogen, J., 1996, Redistribution of rare earth elements, thorium, and uranium over accessory minerals in the course of amphibolite to granulite facies metamorphism: The role of apatite and monazite in orthogneisses from southwestern Norway: Geochimica et Cosmochimica Acta, v. 60, n. 8, p. 1341–1354, doi:10.1016/0016-7037(96)00006-3.

Bouvier, A., Vervoort, J. D., and Patchett, P. J., 2008, The Lu-Hf and Sm-Nd isotopic composition of CHUR: Constraints from unequilibrated chondrites and implications for the bulk composition of terrestrial planets: Earth and Planetary Science Letters, v. 273, n. 1–2, p. 48–57, doi:10.1016/j.epsl.2008.06.010.

Chappell, B. W., 1999, Aluminium saturation in I- and S-type granites and the characterization of fractionated haplogranites: Lithos, v. 46, n. 3, p. 35–551, doi:10.1016/S0024-4937(98)00086-3.

Chappell, B. W., and White, A. J. R., 1974, Two contrasting granite types: Pacific Geology, v. 8, p. 173–174.

Corfu, F., Hanchar, J. M., Hoskin, P. W. O., and Kinny, P., 2003, Atlas of zircon textures: Reviews in Mineralogy and Geochemistry, v. 53, n. 1, p. 469–500, doi:10.2113/0530469.

Dörr, W., and Zulauf, G., 2010, Elevator tectonics and orogenic collapse of a Tibetan-style plateau in the European Variscides: The role of the Bohemian shear zone: International Journal of Earth Sciences, v. 99, n. 2, p. 299–325, doi:10.1007/s00531-008-0389-x.

Dudauri, O. Z., Togonidze, M. G., and Vashakidze, G. T., 1990, K-Ar age of the granitoids of the Transcaucasian median massif: Freiberger Forschungshefte, Isotope und Umweltschutz, p. 42–44.

Finger, F., and Broska, I., 1999, The Gemeric S-type granites in southeastern Slovakia: Late Palaeozoic or Alpine intrusion? Evidence from electron-microprobe dating of monazite: Schweizerische mineralogische und petrographische Mitteilungen, v. 79, p. 439–443.

Finger, F., and Krenn, E., 2007, Three metamorphic monazite generations in a high-pressure rock from the Bohemian Massif and the potentially important role of apatite in stimulating polyphase monazite growth along a PT loop: Lithos, v. 95, n. 1–2, p. 103–115, doi:10.1016/j.lithos.2006.06.003.

Finger, F., and Von Quadt, A., 1995, U-Pb ages of zircons from a plagiogranite-gneiss in the south-eastern Bohemian massif, Austria: further evidence for an important early Paleozoic rifting episode in the eastern Variscides: Schweizerische mineralogische und petrographische Mitteilungen, v. 75, p. 265–270.

Finger, F., Gerdes, A., Janousek, V., René, M., and Riegler, G., 2007, Resolving the Variscan evolution of the Moldanubian sector of the Bohemian Massif: the significance of the Bavarian and the Moravo-Moldanubian tectonometamorphic phases: Journal of Geosciences, v. 52, n. 1–2, p. 9–28, doi:10.3190/jgeosci.005.

Floyd, P. A., and Winchester, J. A., 1975, Magma type and tectonic setting discrimination using immobile elements: Earth and Planetary Science Letters, v. 27, n. 2, p. 211–218, doi:10.1016/0012-821X(75)90031-X.

Franke, W., 2000, The mid-European segment of the Variscides; tectonostratigraphic units, terrane boundaries and plate tectonic evolution, *in* Franke W., Haak V., Oncken O., and Tanner D., editors, Orogenic Processes: Quantification and Modelling in the Variscan Belt: Geological Society, London, Special Publications, v. 179, p. 35–61, doi:10.1144/GSL.SP.2000.179.01.05.

Friedl, G., Finger, F., McNaughton, N. J., and Fletcher, I. R., 2000, Deducing the ancestry of terranes: SHRIMP evidence for South America-derived Gondwana fragments in central Europe: Geology, v. 28, n. 11, p. 1035–1038, doi:10.1130/0091-7613(2000)28⟨1035:DTAOTS⟩2.0.CO;2.

Frost, R. B., Barnes, C. G., Collins, W. J., Arculus, R. J., Ellis, D. J., and Frost, C. D., 2001, A geochemical classification for granitic rocks: Journal of Petrology, v. 42, n. 11, p. 2033–2048, doi:10.1093/petrology/42.11.2033.

Gamkrelidze, I. P., 1986, Geodynamic evolution of the Caucasus and adjacent areas in Alpine time: Tectonophysics, v. 127, n. 3–4, p. 261–277, doi:10.1016/0040-1951(86)90064-8.

——— 1991, Tectonic nappes and horizontal layering of the Earth's crust in the Mediterranean belt (Carpathians, Balkanides and Caucasus): Tectonophysics, v. 196, n. 3–4, p. 385–396, doi:10.1016/0040-1951(91)90332-M.

——— 1997, Terranes of the Caucasus and adjacent areas: Bulletin of the Georgian Academy of Sciences, v. 155, p. 75–81.

Gamkrelidze, I., and Shengelia, D., 1999, Magmatites of the Dzirula Crystalline Massif in the Light of Tectonic Layering of the Earth's Crust: Bulletin of the Georgian Academy of Science, v. 159, p. 117–120.

——— 2001, Origin of the Igneous Rocks of the Dzirula Crystalline massif (Caucasus) in light of the tectonic layering of the Earth's crust: Geotectonics, v. 35, n. 1, p. 51–61.

Gamkrelidze, I., Shengelia, D., Shvelidze, I. U., and Vashakidze, G. T., 1999, The new data about geological structure of the Lokhi crystalline massif and Gorastskali metaophiolites: Proceedings of Geological Institute of Academy of Sciences, Georgia, New Series v. 114, p. 82–108.

Gamkrelidze, I. P., Dudauri, O. Z., Nadareishvili, G. Sh., Skhirtladze, N. i., Tutberidze, B. D., and Shengelia, D., 2002, Geodynamic typification of Precambrian-Phanerozoic magmatism of Georgia: Proceedings of the A. Janelidze Geological Institute of the Georgian Academy of Sciences, New Series, v. 117, p. 105–126.

Gerdes, A., and Zeh, A., 2006, Combined U-Pb and Hf isotope LA-(MC-)ICP-MS analyses of detrital zircons: Comparison with SHRIMP and new constraints for the provenance and age of an Armorican metasediment in Central Germany: Earth and Planetary Science Letters, v. 249, p. 47–61, n. 1–2, doi:10.1016/j.epsl.2006.06.039.

——— 2009, Zircon formation versus zircon alteration—new insights from combined U-Pb and Lu-Hf in-situ La-ICP-MS analyses, and consequences for the interpretation of Archean zircon from the Central Zone of the Limpopo Belt: Chemical Geology, v. 261, p. 230–243, doi:10.1016/j.chemgeo.2008.03.005.

Ghukasiayn, R., and Somin, M., 1995, Rb-Sr isochron dating of metamorphic rocks of the Main Range zone, *in* Main problems of geological investigation and mineral resources of the North Caucasus, Materials of VIII conference: Essentuki. p. 239–240 (in Russian).

Golonka, J., 2004, Plate tectonic evolution of the southern margin of Eurasia in the Mesozoic and Cenozoic: Tectonophysics, v. 381, n. 1–4, p. 235–273, doi:10.1016/j.tecto.2002.06.004.

Hanel, M., Lippold, H. J., Kober, B., Gurbanov, A. G., and Borsuk, A. M., 1993a, Isotope-geochemical reconstruction of the primary nature of volcanites in metamorphic complexes of the Great Caucasus (with reference to the Buul'gen and Makera Groups): Petrology 1, v. 2, p. 143–158.

——— 1993b, On the Early Paleozoic age of metagranodiorites in the Main Range zone of the Greater Caucasus: Petrology 1, v. 5, p. 487–498.

Heinrich, W., Andrehs, G., and Franz, G., 1997, Monazite-xenotime miscibility gap thermometry: I. An empirical calibration: Journal of Metamorphic Geology, v. 15, p. 3–16, doi:10.1111/j.1525-1314.1997.t01-1-00052.x.

Henk, A., von Blankenburg, F., Finger, F., Schaltegger, U., and Zulauf, G., 2000, Syn-convergent high-temperature metamorphism and magmatism in the Variscides—a discussion of potential heat sources: Geological Society, London, Special Publications, v. 179, p. 387–399, doi:10.1144/GSL.SP.2000.179.01.23.

Janousek, V., Gerdes, A., Vrána, S., Finger, F., Erban, V., Friedl, G., and Braithwaite, C. J. R., 2006, Low-pressure granulites of the Lisov Massif, Southern Bohemia: Viséan metamorphism of Late Devonian plutonic arc rocks: Journal of Petrology, v. 47, n. 4, p. 705–744, doi:10.1093/petrology/egi091.

Jarvis, K. E., and Williams, J. G., 1993, Laser ablation inductively coupled plasma mass spectro-metry (LA-ICP-MS): a rapid technique for the direct, quantitative-determination of major, trace and rare-earth elements in geological samples: Chemical Geology, v. 106, p. 251–262, doi:10.1016/0009-2541(93)90030-M.

Kazmin, V. G., 2006, Tectonic Evolution of the Caucasus and Fore-Caucasus in the Late Paleozoic: Doklady Adademii Nauk, v. 406, n. 1, p. 66–68, doi:10.1134/S1028334X06010016.

Krenn, E., Ustaszewski, K., and Finger, F., 2008, Detrital and newly formed metamorphic monazite in amphibolite-facies metapelites from the Motajica Massif, Bosnia: Chemical Geology, v. 254, n. 3–4, p. 164–74, doi:10.1016/j.chemgeo.2008.03.012.

Ludwig, K. R., 2000, Users manual for Isoplot/Ex version 2.2: a geochronological toolkit for Microsoft Excel: Berkeley Geochronology Center Special publication 1A.

Mehnert, K. R., 1968, Migmatites and the Origin of Granitic Rocks: New York, Elsevier, 393 p.

Moix, P., Beccaletto, L., Kozur, H. W., Hochard, C., Rosselet, F., and Stampfli, G. M., 2008, A new classification of the Turkish terranes and sutures and its implication for the paleotectonic history of the region: Tectonophysics, v. 451, p. 7–39, doi:10.1016/j.tecto.2007.11.044.

Montel, J. M., Foret, S., Veschambrem, M., Nicollet, C., and Provost, A., 1996, Electron microprobe dating of monazite: Chemical Geology, v. 131, n. 1–4, p. 37–53, doi:10.1016/0009-2541(96)00024-1.

O'Brien, P., J., 2000, The fundamental Variscan Problem: high-temperature metamorphism at different depths and high-pressure metamorphism at different temperatures, *in* Franke, W., Haak, V., Onken, O., and Tanner, D., editors, Orogenic Pocesses: quantification and modelling in the Variscan Belt: Geological Society, London, Special Publications, v. 179, p. 369–386, doi:10.1144/GSL.SP.2000.179.01.22.

Okrostsvaridze, A. V., Clarke, D., and Reynolds, P., 2002, Sm-Nd, Rb-Sr and K-Ar isotope system and geochemistry and geochronology age of the pre-Alpine granitoids of Dzirula salient of the Caucasian median massif: Georgian Academy of Science, A. Janelidze Geological Institute Proceedings, New series, v. 117, p. 173–186.

Pearce, J. A., 1983, Role of the sub-continental lithosphere in magma genesis at active continental margins, *in* Hawkesworth, C. J., and Norry, M. J., editors., Continental basalts and mantle xenoliths: London, Shiva, Orpington, and Cambridge, Massacuhestts, Birkhauser Boston, p. 230–249.

Pearce, J. A., Harris, N. B., and Tindle, A. G., 1984, Trace element discrimination diagrams for the tectonic interpretation of granitic rocks: Journal of Petrology, v. 25, n. 4, p. 956–983, doi:10.1093/petrology/25.4.956.

Perchuk, A., and Philippot, P., 1997, Rapid cooling and exhumation of eclogitic rocks from the Great Caucasus: Journal of Metamorphic Geology, v. 15, n. 3, p. 299–310, doi:10.1111/j.1525-1314.1997.00022.x.

Petrik, I., and Broska, I., 1994, Petrology of two granite types from the Tribeč Mountains, Western Carpathians; an example of allanite (+ magnetite) versus monazite dichotomy: Geological Journal, v. 29, p. 59–78, doi:10.1002/gj.3350290106.

Philippot, P., Blichert-Toft, J., Perchuk, A., Costa, S. and Gerasimov, V., 2001, Lu-Hf and Ar-Ar chronometry supports extreme rate of subduction zone metamorphism deduced from geospeedometry: Tectonophysics, v. 342, n. 1–2, p. 23–38, doi:10.1016/S0040-1951(01)00155-X.

Pyle, J. M., Spear, F. S., Rudnick, R. L., and McDonough, W. F., 2001, Monazite-xenotime garnet equilibrium in metapelites and a new monazite-garnet thermometer: Journal of Petrology. v. 42, n. 11, p. 2083–2107, doi:10.1093/petrology/42.11.2083.

Roberts, M. P., and Clemens, J. D., 1993, Origin of high-potassium, calc-alkaline I-type granitoids: Geology, v. 21, n. 9, p. 825–828, doi:10.1130/0091-7613(1993)021⟨0825:OOHPTA⟩2.3.CO;2.
Schaltegger, U., and Brack, P., 2007, Crustal-scale magmatic systems during intracontinental strike-slip tectonics: U, Pb and Hf isotopic constraints from Permian magmatic rocks of the Southern Alps: International Journal of Earth Sciences, v. 96, n. 6, p. 1131–1151, doi:10.1007/s00531-006-0165-8.
Schulmann, K., Kröner, A., Hegner, E., Wendt, I., Konopásek, J., Lexa, O., and Štípská, P., 2005, Chronological constraints on the pre-orogenic history, burial and exhumation of deep-seated rocks along the eastern margin of the Variscan Orogen, Bohemian Massif, Czech Republic: American Journal of Sciences, v. 305, p. 407–448, doi:10.2475/ajs.305.5.407.
Siebel, W., Shang, C. K., Reitter, E., Rohrmüller, J., and Breiter, K., 2008, Two distinctive granite suites in the SW Bohemian Massif and their record of emplacement: Constraints from geochemistry and zircon $^{207}Pb/^{206}Pb$ chronology: Journal of Petrology, v. 49, n. 10, p. 1853–1872, doi:10.1093/petrology/egn049.
Somin, M. L., Kotov, A. B., Sal'nikova, E. B., Levchenkov, O. A., Pis'mennyi, A. N., and Yakovleva, S. Z., 2006, Paleozoic rocks in infrastructure of the metamorphic core, the Greater Caucasus Main range zone: Stratigraphy and Geological Correlation, v. 14, p. 475–485, doi:10.1134/S0869593806050029.
Somin, M. L., Lepekhina, E. N., and Konilov, A. N., 2007, Age of the High-Temperature Gneiss Core of the Central Caucasus: Doklady Earth Sciences, v. 415, n. 1, p. 690–694, doi:10.1134/S1028334X07050066.
Spear, F. S., Kohn, M. J., and Cheney, J. T., 1999, P-T paths from anatectic pelites: Contributions to Mineralogy and Petrology, v. 134, n. 1, p. 17–32, doi:10.1007/s004100050466.
Stacey, J. S., and Kramers, J. D., 1975, Approximation of terrestrial lead isotope evolution by a two-stage model: Earth and Planetary Science Letters, v. 26, n. 2, p. 207–221, doi:10.1016/0012-821X(75)90088-6.
Stampfli, G. M., and Borel, G. D., 2002, A plate tectonic model for the Paleozoic and Mesozoic constrained by dynamic plate boundaries and restored synthetic oceanic isochrons: Earth and Planetary Science Letters, v. 196, p. 17–33, doi:10.1016/S0012-821X(01)00588-X.
Sun, S. S., and McDonough, W. F., 1989, Chemical and isotopic systematics of oceanic basalts: Implications for mantle composition and process, *in* Saunders, A. D., and Norry, M. J., editors, Magmatism in the Ocean Basins: Geological Society, London, Special Publications, v. 42, p. 313–345, doi:10.1144/GSL.SP.1989.042.01.19.
Tarney, J., and Jones, C. E., 1994, Trace-element geochemistry of orogenic igneous rocks and crustal growth-models: Journal of the Geological Society, London, v. 151, n. 5, p. 855–868, doi:10.1144/gsjgs.151.5.0855.
Timmermann, H., Dörr, W., Krenn, E., Finger, F., and Zulauf, G., 2006, Conventional and in situ geochronology of the Teplá Crystalline unit, Bohemian Massif: implications for the processes involving monazite formation: International Journal of Earth Science, v. 95, n. 4, p. 629–647, doi:10.1007/s00531-005-0060-8.
Topuz, G., Altherr, R., Schwartz, W. H., Dokuz, A., and Meyer, H.-P., 2007, Variscan amphibolite-facies rocks from the Kurtoglu metamorphic complex (Gümüşhane area, Eastern Pontides, Turkey): International Journal of Earth Science, v. 96, n. 5, p. 861–873, doi:10.1007/s00531-006-0138-y.
Topuz, G., Altherr, R., Siebel, W., Schwarz, W. H., Zack, T., Hasözbek, A., Barth, M., Satir, M., and Şen, C., 2010, Carboniferous high-potassium I-type granitoid magmatism in the Eastern Pontides: the Gümüşhane pluton (NE Turkey): Lithos, v. 116, n. 1–2, p. 92–110, doi:10.1016/j.lithos.2010.01.003.
Tropper, P., Deibl, I., Finger, F., and Kaindl, R., 2006, P-T-t evolution of spinel-cordierite-garnet gneisses from the Sauwald Zone (Southern Bohemian Massif, Upper Austria): Is there evidence for two independent late-Variscan low-P/high-T events in the Moldanubian Unit?: International Journal of Earth Science, v. 95, n. 6, p. 1019–1037, doi:10.1007/s00531-006-0082-x.
Tsutsunava, T., 2002, About primary rocks of metamorphites of Chorchana-Utslevi allochthonous complex of the Dzirula crystalline massif: Proceedings of the A. Janelidze Geological Institute of the Georgian Academy of Sciences, New Series, v. 117, p. 187–194.
Von Raumer, J. F., and Stampfli, G. M., 2008, The birth of the Rheic Ocean–Early Palaeozoic subsidence patterns and subsequent tectonic plate scenarios: Tectonophysics, v. 461, n. 1–4, p. 9–20, doi:10.1016/j.tecto.2008.04.012.
Von Raumer, J. F., Stampfli, G. M., and Bussy, F., 2003, Gondwana-derived microcontinents—the constituents of the Variscan and Alpine collisional orogens: Tectonophysics, v. 365, n. 1–4, p. 7–22, doi:10.1016/S0040-1951(03)00015-5.
Williams, M. L., Jercinovic, M. J., Goncalves, P., and Manhan, K., 2006, Format and philosophy for collecting, compiling, and reporting microprobe monzite ages: Chemical Geology, v. 225, p. 1–15, doi:10.1016/j.chemgeo.2005.07.024.
Winchester, J. A., Pharaoh, T. C., and Verniers, J., 2002, Palaeozoic amalgamation of Central Europe. An introduction and synthesis of new results from recent geological and geophysical investigations, *in* Winchester, J. A., Pharaoh, T. C., and Verniers, J., editors, Palaeozoic amalgamation of Central Europe: Geological Society, London, Special Publications, v. 201, p. 1–18, doi:10.1144/GSL.SP.2002.201.01.01.
Yilmaz, A., Adamia, S., Chabukiani, A., Chkhotua, T., Erdoğan, K., Tuzcu, S., and Karabiyikoğlu, M., 2000, Structural correlation of the southern Transcaucasus (Georgia)–eastern Pontides (Turkey), *in* Bozkurt, E., Winchester, J. A., and Piper, J. D. A., editors, Tectonics and Magmatism in Turkey and Surrounding Area: Geological Society, London, Special Publications, v. 173, p. 171–182, doi:10.1144/GSL.SP.2000.173.01.08.
Zakariadze, G. S., Karpenko, S. F., Bazylev, B. A., Adamia, S. A., Oberhansli, R. E., Solov'eva, N. V., and Lyalikov, A. V., 1998, Petrology, geochemistry and Sm-Nd age of the pre-Late Hercynian paleooceanic complex of the Dzirula salient, Transcaucasian massif: Petrology, v. 6, p. 388–408.
Zakariadze, G. S., Dilek, Y., Adamia, S. A., Oberhänsli, R. E., Karpenko, S. F., Bazylev, B. A., and Solov'eva, N. V., 2007, Geochemistry and geochronology of the Neoproterozoic Pan-African Transcaucasian

Massif (Republic of Georgia) and implications for island arc evolution of the late Precambrian Arabian-Nubian Shield: Gondwana Research, v. 11, n. 1–2, p. 92–108.

Zulauf, G., 1997, Von der Anchizone bis zur Eklogitfazies: Angekippte Krustenprofile als Folge der cadomischen und variscischen Orogenese im Teplá-Barrandium (Böhmische Masse): Geotektonische Forschungen, v. 89, p. 1–302.

Zwart, H. J., and Dornsiepen, U. F., 1980, The Variscan and pre-Variscan tectonic evolution of Central and Western Europe: a tentantive model: Memoires du Bureau de Recherches Geologiques et Minieres, v. 168, p. 226–232.